AD-A076 155 ARMY ELECTRONICS RESEARCH AND DEVELOPMENT COMMAND FO--ETC F/G 9/5
OVERVIEW OF PULSE-HEIGHT ANALYSIS OF IMAGE INTENSIFIER TUBES.(U)
JUN 79 B H AHN

UNCLASSIFIED DELNV-TR-0006 NL

1 OF 1
AD A076155

END
DATE FILMED
11-79
DDC

(12) LEVEL II

AD

AD A076155

(14) Report DELNV-TR-0006

(6) OVERVIEW OF PULSE-HEIGHT ANALYSIS OF IMAGE INTENSIFIER TUBES,

(9) Final rept. Nov 77 - Sep 78,

by

(10) Byong H. Ahn

(11) June 1979

(12) 65

Approved for public release; distribution unlimited.

393 889

U.S. ARMY ELECTRONICS R&D COMMAND
NIGHT VISION & ELECTRO-OPTICS LABORATORY
FT. BELVOIR, VIRGINIA 22060

Destroy this report when no longer needed.
Do not return it to the originator.

The citation in this report of trade names of commercially available products does not constitute official endorsement or approval of the use of such products.

UNCLASSIFIED

SECURITY CLASSIFICATION OF THIS PAGE (When Data Entered)

REPORT DOCUMENTATION PAGE		READ INSTRUCTIONS BEFORE COMPLETING FORM
1. REPORT NUMBER DELNV-TR-0006	2. GOVT ACCESSION NO.	3. RECIPIENT'S CATALOG NUMBER
4. TITLE (and Subtitle) OVERVIEW OF PULSE-HEIGHT ANALYSIS OF IMAGE INTENSIFIER TUBES		5. TYPE OF REPORT & PERIOD COVERED Final Report November 1977-September 1978 6. PERFORMING ORG. REPORT NUMBER
7. AUTHOR(s) Byong H. Ahn		8. CONTRACT OR GRANT NUMBER(s)
9. PERFORMING ORGANIZATION NAME AND ADDRESS Night Vision & Electro-Optics Laboratory Fort Belvoir, VA 22060		10. PROGRAM ELEMENT, PROJECT, TASK AREA & WORK UNIT NUMBERS
11. CONTROLLING OFFICE NAME AND ADDRESS Night Vision & Electro-Optics Laboratory Fort Belvoir, VA 22060		12. REPORT DATE June 1979 13. NUMBER OF PAGES 67
14. MONITORING AGENCY NAME & ADDRESS(if different from Controlling Office)		15. SECURITY CLASS. (of this report) Unclassified 15a. DECLASSIFICATION/DOWNGRADING SCHEDULE

16. DISTRIBUTION STATEMENT (of this Report)

Approved for public release; distribution unlimited.

17. DISTRIBUTION STATEMENT (of the abstract entered in Block 20, if different from Report)

18. SUPPLEMENTARY NOTES

19. KEY WORDS (Continue on reverse side if necessary and identify by block number)

Image Intensifier Tube	Pulse-Height Analysis
Multiple-Channel Analyzer	Microchannel Plate
Wide-Gap Diode	Photoemission
Photocathode	Phosphor Screen

20. ABSTRACT (Continue on reverse side if necessary and identify by block number)

Pulse-height analysis (PHA) of image intensifier tubes (I^2 tube) is described using a multiple-channel analyzer (MCA). The experimental setup, schematics of I^2 tubes, statistics and mathematics for the anlaysis, and methods for data acquisition and reduction are included in the report.

PHA complements another experimental technique which measures the noise figure (N_f) of an I^2 tube by explaining causes for good or bad performance of the tube.

(Continued)

DD FORM 1 JAN 73 1473 EDITION OF 1 NOV 65 IS OBSOLETE

UNCLASSIFIED

SECURITY CLASSIFICATION OF THIS PAGE (When Data Entered)

(Block 20. (Cont'd))

Technical developments of I^2 tubes over the years were retraced to point out the improvements or the distinctions of a later generation I^2 tube over an earlier one. Some of the tube characteristics are described in detail when they affect the N_F or the gain noise figure.

Background mathematics and statistics are illustrated, and some useful oscilloscope traces are given for reference in Appendix B.

PREFACE

This work was accomplished under the direction of Mr. Charles Freeman, Director, EODD. Dr. Herbert Pollehn offered technical advice throughout the work. He also read the manuscript very carefully and made numerous suggestions to make this report a technically better one.

Mr. Ray Stefanik arranged the experimental setup and the calibration of the instruments; Mr. Robert Feingold programmed the computer routine; and Mr. William Gutiurez supplied information on the growth of GaAs photocathode.

Mr. James E. Miller and Mr. William Dateno reviewed the manuscript to make it more readable.

ILLUSTRATIONS

ILLUSTRATIONS (Cont'd)

TABLES

OVERVIEW OF PULSE-HEIGHT ANALYSIS OF IMAGE INTENSIFIER TUBES

I. Introduction. This report deals with the pulse-height analysis (PHA) of an image intensifier tube using a multiple-channel analyzer (MCA). The experimental setup, the schematics of the tubes, statistics and mathematics for the analysis, and methods for data acquisition and data reduction are included in the report.

This report is aimed primarily at those who do not have a background in PHA and/or knowledge of the tubes. Many experimental results are included as reminders that they have already been obtained. This is to prevent the re-invention of the wheel. Description of the tubes should be regarded as general. However, the knowledge of the basic tube technology is helpful in performing the PHA.

The PHA is concerned with the scintillation (pulse height or pulse energy) distribution of a tube. The scintillations are generated by electrons of numerous origins. Photoelectrons, thermal electrons, and photocathode electrons generated by ion bombardment are some of the important kinds of electrons discussed here.

The PHA is intended to complement another experimental technique which measures the noise figure (N_F) of a tube. N_F is defined as the ratio of the signal-to-noise ratio (S/N) at the output of the photocathode to the signal-to-noise ratio at the output of the phosphor screen. N_F is an important parameter of a tube's performance. The detection range of a tube is inversely proportional to N_F.

The PHA can provide some of the answers regarding the noise characteristics of a tube. Study of a pulse-height distribution provides information as to the secondary emission process of a microchannel plate (MCP), the fabrication processes of the tube components, and the assembly technique of the tube.

Even though an end item of PHA, the gain noise figure N_{FG} is proportional to the noise figure N_F by $N_F = \frac{1}{\sqrt{D}} N_{FG}$, where D is the detection probability. The magnitude of N_{FG} should not be confused with the magnitude of N_F because D is a complicated variable.

The interpretation of the PHA must be judicious. The results of the PHA do not mean much unless they are correlated with other physical parameters of the tube.

Two main references for this report are:

Photomultiplier Manual, by RCA, 1970.

"Photo-Electronic Image Devices," 6th Symposium Proceedings held at London Imperial College, London, 9-13 September 1974, Academic Press, London, 1976.

The manual explains the statistics behind PHA and is recommended for those who have no previous experience in this field. The symposium proceedings are useful for an understanding of the physics of PHA.

II. Setup. The experimental setup of PHA in pulse-height mode is shown in Figure 1.

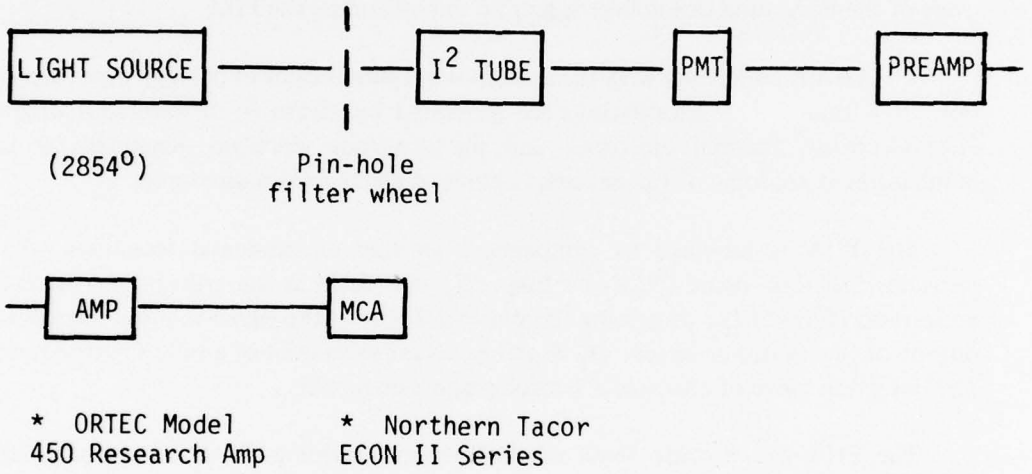

Figure 1. Experimental set-up of PHA in pulse height mode.

Light from a lamp is focused onto a tube. The flux is controlled by a pin-hole wheel (a wheel with various size holes) and a neutral-density filter wheel. A beam of almost 2 mm in diameter is directed on the photocathode by means of a light pipe and an optical system after the light flux is controlled. The input light level is required to be low in some setups to maintain low probability of coincident events.

The photocathode (P.C.) of a tube converts photons into electrons. The electrons are given high kinetic energy and/or multiplied and sent toward the phosphor screen (screen).

The output of the tube (scintillations) is picked up by a photomultiplier tube (PMT), amplified, and fed into a multichannel analyzer (MCA). Each scintillation from the screen has a finite width and finite height, the value of which corresponds

proportionally to the visual perception of a bright or a weak scintillation. The brightness depends upon the number and energy of electrons arriving at a screen site simultaneously. The number of electrons is dependent on the multiplication mechanism of the tube. If a single electron from the P.C. causes the scintillation at the screen, the scintillation is referred to as a single-electron pulse scintillation. If multiple electrons from P.C. cause the scintillation, it is referred to as a multiple-electron pulse scintillation.

PHA can be obtained by two methods: the pulse-height mode and the pulse-integration mode. The pulse-height mode assumes that the pulse energy is represented by its height. The pulse-integration mode integrates the pulse for a given time period, which is arbitrary but is designed so that most of the area of the large pulses is integrated. This mode takes care of the variation in the pulse widths and is the most realistic and accurate experiment if used judiciously. The mode requires careful calibration procedures to insure its proper use. The discriminator (see Appendix A) determines the low-energy electron population, which in turn affects the total population a great deal because the low-energy electron population comprises most of the experimental population.

The experimental results of this report are obtained by the pulse-height mode. This mode is fairly accurate and is experimentally proved to be equivalent to the pulse-integration mode for higher energy pulses. This is because the decay time constant of the pulse is essentially determined by the phosphor decay time, and it is independent of the pulse height. This means the area under the curve is proportional to the height only.

An MCA linearly converts pulse heights into channel numbers and displays it in the pulse-height mode.

The necessary data are collected in two sets: Set I and Set II. Set I is used as the basis for the normalization and the data reduction of Set II. The data-reduction method is such that the data of various I^2 tubes are directly compared even though the experimental conditions and the gain are different from each other. This will be explained more in a later section.

III. Image Intensifier Tube. Three technical development stages of the tube are generally acknowledged. Only the important technical features of the first and second generation tubes will be mentioned. A third generation tube (3rd gen tube) is the most recent tube.

A. The 1st Gen Tube. The primary means of intensification of the incoming signal is by supplying high kinetic energy to the photoelectrons. Since this gain is on the order of 100, several tubes are coupled to obtain a high gain. An earlier version of a 3-stage tube is illustrated in Figure 2.[1]

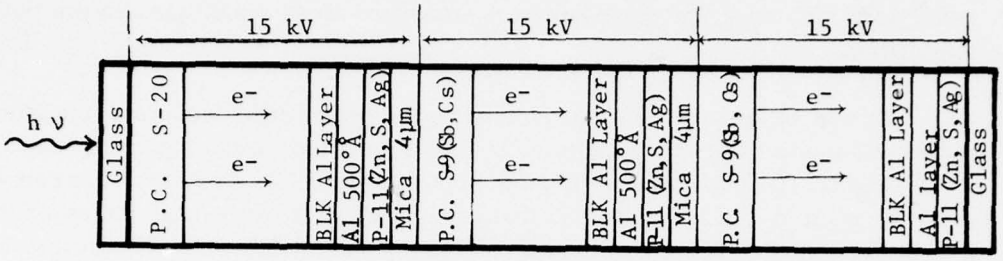

Figure 2. First gen tube.

The first photocathode is designed to respond well to the infrared spectra, and the subsequent photocathodes are matched to the P-11 phosphor. With the three stages, the overall gain is as high as 10^6. Note that this tube has black Al layers as AR coatings for the light which passes through the photocathode. The black Al layer is formed when Al is evaporated at poor vacuum (0.2 torr). The Al layer on the phosphor screen prevents positive ions from travelling toward P.C.

Now, the phosphor screen is so well scrubbed that ion feedback is no longer a problem. But instead it is mainly used as an anti-reflecting coating for the light which passes through. A later version of a 1st gen, 3-stage tube is given in Figure 3.

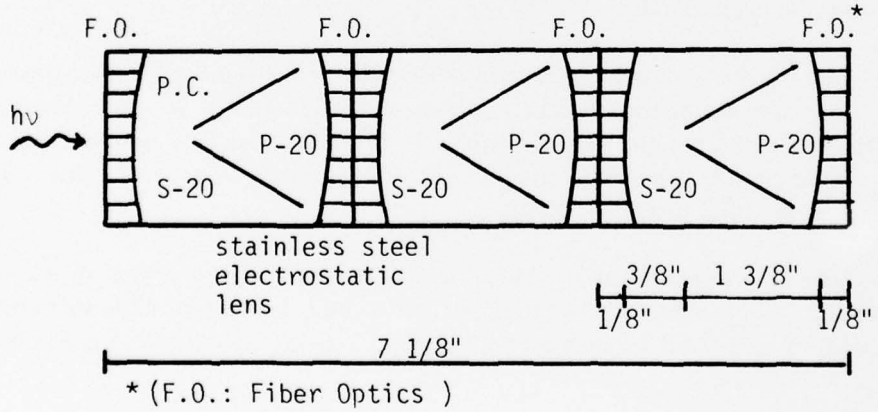

Figure 3. First gen inverter tube.

[1] J. D. McGee, R. W. Airey, and M. Aslam, "Adv. in E. E. P.," Vol. 22. p. 571 (1966).

The white-light gain is 100 for the 1st stage and about 40 per stage in the subsequent stages. Therefore, the total gain can be almost 1.6×10^5. The curved photocathode improves the edge resolution and prevents the image from being distorted. The electrons land on the curved P-20 whose curvature follows the image plane of the electron images arriving at the phosphor screen. The images are still inverted after going through three stages due to the image inversion by each stainless steel electrostatic lens but with the collecting-optics inversion the image is right-side up. The stainless steel cone acts as the ion deflector: due to the large mass of the ions, the path of the off-axis ions cannot be bent enough for these ions to go through the hole in the stainless steel except the axial ions. In this type of a tube, the maximum attainable gain is sacrificed in exchange for the simplification of production complexity by making one type of stage only in comparison to the previous example.

The 1st gen tubes are bulky ($\cong$7 inches long) and require high voltages ($\simeq$ 45 kV for three stages), but they are quiet in comparison to the subsequent generation tubes.

The concept of a cascade system like the 1st gen tube may come into vogue again in conjunction with a search for low-cost tubes.

B. The 2nd Gen Tube. A 2nd gen tube intensifies the incoming signal by use of an MCP. The electron gain is obtained by the secondary emission of electrons inside the MCP. Because of the MCP, a compact-sized tube is obtained with a suitable gain. Since the 3rd gen tube is very similar to the 2nd gen tube except for the photocathode, it will be described in detail, and further description of a 2nd gen tube will be omitted except as a schematic of a tube. Figure 4 illustrates a typical 2nd gen electrostatic inverter I^2 tube. (There is also a 2nd gen wafer tube without an electrostatic lens, and it is different from a 3rd gen tube in the photocathode and the secondary emission material in MCP).

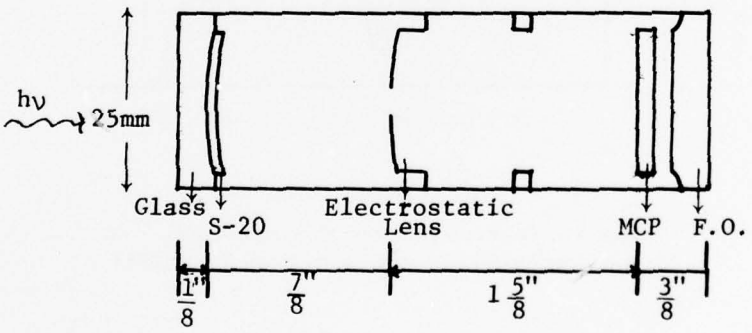

Figure 4. Second gen tube.

The curved photocathode and the electrostatic lens with its ion-trapping capability are carried over from the 1st gen tube. But the MCP is used for the electron gain. Approximate net voltage drop for the photoelectron to the MCP is about 3 kV, 600 V across the MCP, and 6 kV across the screen and the end of the MCP. The MCP does not have an Al_2O_3 screen on the input side, and it is not coated with high secondary emission gain material.

C. **The 3rd Gen Tube.** A 2nd gen tube uses a tri-alkali photocathode (S-20) whereas a 3rd gen tube uses a cesiated GaAs photocathode. The quantum efficiency is improved and the detection threshold of the tube is extended with good efficiency (see Figure 5).

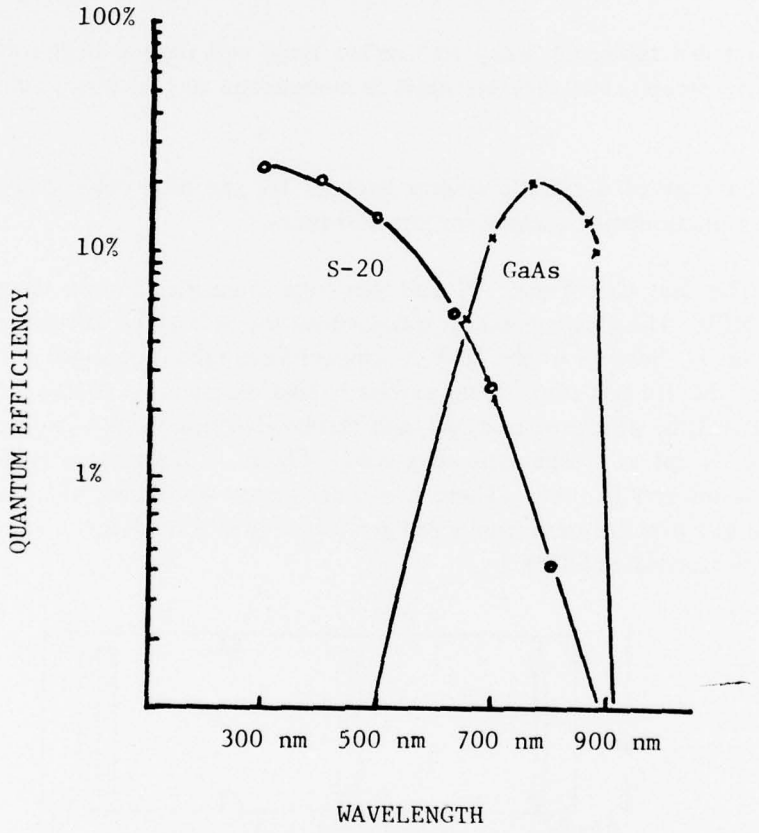

Figure 5. Quantum efficiency of photocathodes. (Transmission Mode) (From a Varian chart, 3773, 1/78.)

Figure 6 illustrates a typical 3rd gen tube.

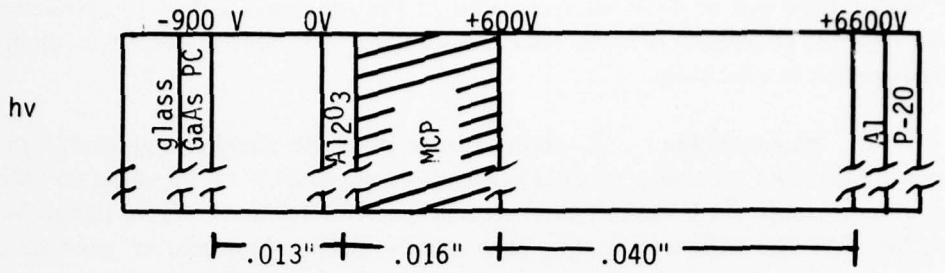

Figure 6. Third gen tube.

Three features are distinctive in comparison to the 1st gen tube:

(1) The system is smaller and lighter, enabling foot-soldier use applications.

(2) Only 7.5 kV is needed in comparison to 45 kV in the 1st gen tube.

(3) The system is noisier than the 1st gen tube (see Table 1).[2]

Table 1. Noise Characteristics of Current Image Intensifiers

Description		Open* Area Ratio	D	N_{FG}**	N_F
1. First Generation, 3-Stage		1.0	0.80	1.20	1.35
2. Second Generation, Inverter		0.6	0.55	1.50	2.00
3. Second Generation, Wafer					
Uncoated MCP***	(i)	0.8	0.80	1.60	1.80
	(ii)	0.6	0.75	1.60	1.80
Coated MCP***, High-Current Scrub		0.6	0.30	1.50	2.70
Coated MCP***, Low-Current Scrub	(i)	0.8	0.70	1.50	1.80
	(ii)	0.6	0.55	1.50	2.00

* Open area ratio is the ratio of the open pore of the MCP to the closed area (claddings).

** Note that N_{FG} is not synonymous with N_F.

*** Coated or uncoated means Al_2O_3 layer at the input of MCP.

(from H. Pollehn, *et al.*, "Adv. in E.E.P.," Vol. 40A, p. 24 (1976).)

[2] H. Pollehn, *et al.*, "Adv. in E.E.P.," Vol. 40A, p. 24 (1976).

An I^2 wafer tube will be dealt with in detail in the following section to reveal the possible and known sources of noise and how some of these sources have been eliminated or dealt with effectively.

1. **Photocathode.**[3] A photocathode converts incoming photons into electrons. Quantum efficiency (# of electrons/# of photons) is on the order to 20% in the 700-nm range for a GaAs photocathode and 2.5% for an S-20 (see Figure 5). A photon, if it has sufficient energy, generates an electron-hole pair or pairs (i.e., $n = \frac{h_\upsilon}{E_g}$ where h_υ is the energy of the photon and E_g, the bandgap). The electron is elevated from the valence band to the conduction band. This is termed photoconduction. Further, the conduction electron can escape from the photocathode into the vacuum if it can overcome the binding force called the electron affinity. This is called photoemission.

There are three mechanisms which will reduce the quantum efficiency of a photocathode:

a. The input photons must be absorbed by the photocathode: transmission and reflection reduce the quantum efficiency.

b. The conduction electrons must travel to the photocathode surfaces: free electrons in the conduction band and the phonons (lattice vibration) reduce the efficiency by inelastic scattering.

c. The electrons must overcome the potential barrier at the vacuum interface, i.e., the electron affinity.

A cesiated GaAs photocathode has negative electron affinity:[4] the energy level of the bottom of the conduction band is higher than that of the vacuum level. This will be explained in detail in the following paragraphs.

This phenomenon is brought about by two factors:

a. GaAs is a doped P-type which has its Fermi level near the valence hand. When the photocathode accepts electrons from cesium, the band bends downward so that the filled acceptor level is below the Fermi level (the unfilled acceptor level is above the Fermi level, and the electron emission is a surface phenomenon).

---

[3] *Photomultiplier Manual*, RCA, 1970.

[4] R. L. Bell, *Negative Electron Affinity Devices*, Clarendon Press, Oxford (1973).

b. Cesium forms a dipole moment with the photocathode when it loses an electron to the GaAs (see Figure 7). This further bends the band.

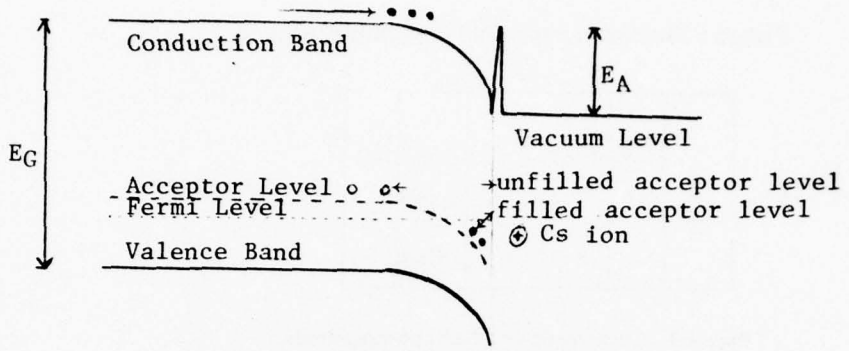

Figure 7. Negative electron affinity band diagram.

Another way of looking at the change of the electron affinity is that the potential developed across the cesium and GaAs interface is the same as the change in electron affinity. The negative electron affinity has a profound effect on the escape probability of the conduction electrons. It explains the increased escape probability of a 3rd gen tube over that of a 2nd gen tube. The decay time of a free electron from above the vacuum level (assuming a positive electron affinity) to the bottom of the conduction band which is below the vacuum level is about 10^{-12} second (see Figure 8). The decay time of a conduction electron from the bottom of the band to the valence band is 10^{-10} second.

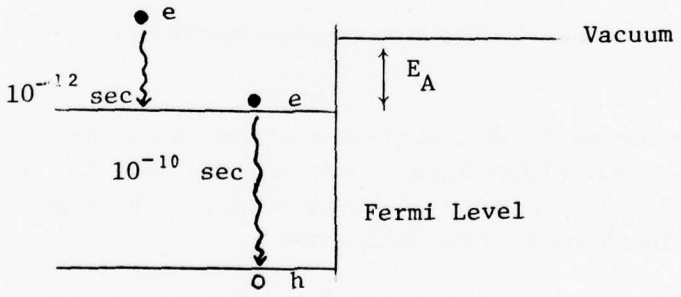

Figure 8. Decay time of a conduction electron.

This implies that an electron of a photocathode with a positive electron affinity has 100 times less of a time period to escape into vacuum than that of a photocathode with a negative electron affinity.

Figure 9 illustrates a typical GaAs photocathode.

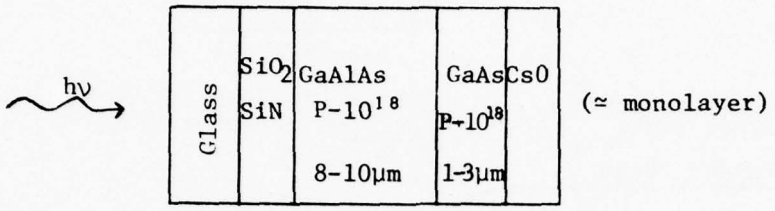

Figure 9. A schematic of a GaAs photocathode.

The glass window transmits only the spectrum with a wavelength longer than 300 nm. SiO_2 and SiN are used to thermal-bond the photocathode to the glass window and as AR coatings. GaAlAs is a passivation layer which prevents the conduction electrons in GaAs from being trapped at the GaAs-glass interface if GaAlAs did not exist (see Figure 10).

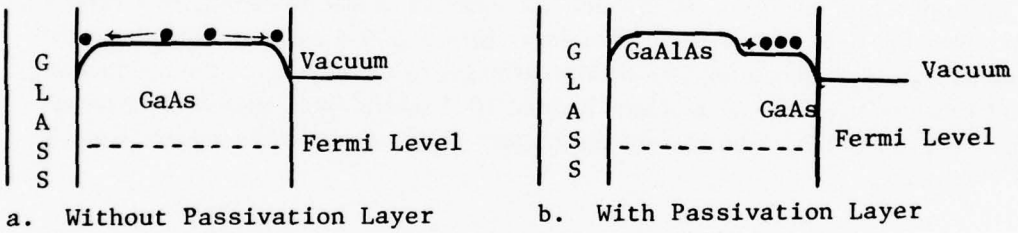

Figure 10. Effect of the passivation layer GaAlAs.

The electron confinement by the passivation is achieved due to the difference in the bandgap. GaAlAs has a larger bandgap than GaAs and with their Fermi levels at the same level, the interface of the conduction bands must be sloped upward as it approaches from the GaAs side to the GaAlAs side.

Figure 11 shows the manner in which a GaAs photocathode is grown on a GaAs substrate.

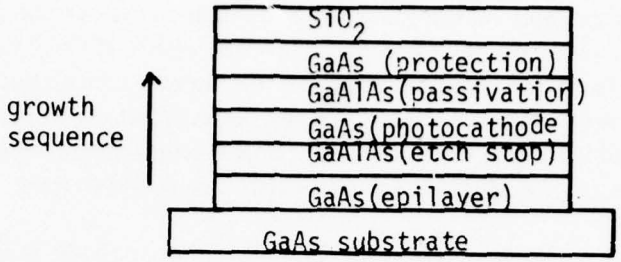

Figure 11. Growth sequence of a GaAs photocathode.

After the growth, GaAs substrate is etched away, stopping at the GaAlAs etch-stop layer. Then, using a GaAlAs etch, the GaAlAs layer is etched away, stopping at the GaAs photocathode layer (some chemicals etch GaAs fast and some, GaAlAs fast. HF etches GaAlAs fast but etches GaAs only negligibly. NaOCl etches GaAs faster than GaAlAs by a factor of three).

After heat-cleaning of the photocathode in vacuum, Cs and 0 are either alternately or simultaneously evaporated onto the GaAs photocathode until the maximum sensitivity is achieved. In the alternating process, since the maximum sensitivity is not known, the evaporation stops after the maximum sensitivity is reached and starts to decline. Then the photocathode is heated until the peak is reached again by evaporating Cs and 0.

Cs is a mysterious but essential element in the photocathode fabrication. However, there is a dearth of information on the behavior of Cs in the photoemission process or on its reactive processes in the tube. It was found that Cs overpressure after the maximum sensitivity is reached is very important to maintain the long lifetime of a photocathode. The overpressure required depends upon whether the photocathode is an S-20 or a GaAs. A GaAs photocathode needs about $10^{-12} - 10^{-14}$ torr (S-20 requires a slightly higher overpressure). The exact pressure is not known. A monolayer of Cs on the cathode (18 mm diameter), if evaporated completely in the tube (5 mm in length), will give a vapor pressure of 10^{-1} torr. Nominally Cs vapor pressure at room temperature is about 10^{-6} torr. Since it is believed that at most a monolayer of Cs exists on the photocathode, it can be argued that one out of 10^{11} Cs atoms participates in the sublimation and the condensation process to maintain the sensitivity.

Cs is a highly reactive element. It can reduce gold oxide. It reacts with glass – even a Pyrex. Cs is a source of ions for the field ion bombardment.

The axial potential gradient in the I^2 tube has enough transverse component to distribute Cs ions and bombard the photocathode. The effect of Cs ion bombardment can be correlated from the experiment where the bright scintillations decrease in number when the tube is cooled down. In the pulse height distribution, it was observed that a cooled wide-gap tube has fewer bright scintillations than a noncooled tube, indicating that the scintillations are only partly due to the Cs ions.

Field emission of electrons from the photocathode is another important source of scintillations. Some scintillations are identified as due to the field emission electrons and some are thought to be due to them. This phenomenon arises because of the surface nonuniformity such as the growth defects and etch defects.

The field strength at the protrusion (a whisker) in evaporated photocathodes is multiplied by a factor shown in Table 2.[5]

Table 2. Experimentally Determined Values of the Field Intensification Factor

Photocathode	Sensitivity ($\mu A\,lm^{-1}$)	Electrode Gap (mm)	Multiplier
S-11	50	1.75	47
Ext. red S-20	195	1.61	40

(after J. A. Cochrane and R. F. Thurmond, "Adv. in E.E.P.," Vol. 40A, p. 441 (1976)).

The scintillation due to field emission is identified as a bright spot on the phosphor screen. It depends upon the potential gradient a photocathode sees regardless of the input light level. This phenomenon is generally referred to as "field emission." The bright spot is referred to as the "emission point." Indentations due to a growth defect (void) or an etching process (usually localized, over-etched spots) can also cause mild forms of field emission: they do not cause the "field emission" phenomenon, but they do cause bright scintillations or the high noise figure.

Obviously this phenomenon or effect depends upon the voltage drop across the photocathode and the subsequent stage: the entrance of an MCP or the phosphor screen if there is no MCP in a tube like a wide-gap diode. In the normal operating mode, an MCP I^2 tube has a voltage drop of 900 V between the photocathode and the entrance of an MCP, a gap of 0.013 inch (0.33 mm). This corresponds to a potential gradient of 2.73 kV/mm. It is observed that the level of bright scintillations increases substantially if the voltage is increased to about 1.4 kV in a 3rd gen tube: this corresponds to 4.24 kV/mm. It is also observed that the level of bright

[5] J. A. Cochrane and R. F. Thurmond, "Adv. in E.E.P.," Vol. 40A, p. 441 (1976).

scintillations in a 2nd gen tube increases suddenly if the voltage is increased to 1000 V where the normal operating voltage is only 800 V. The phenomenon is reversible in a sense that it does not cause a permanent damage to the photocathode. Figure 12 shows the increase in the dark current due to the high field. The sudden increase at

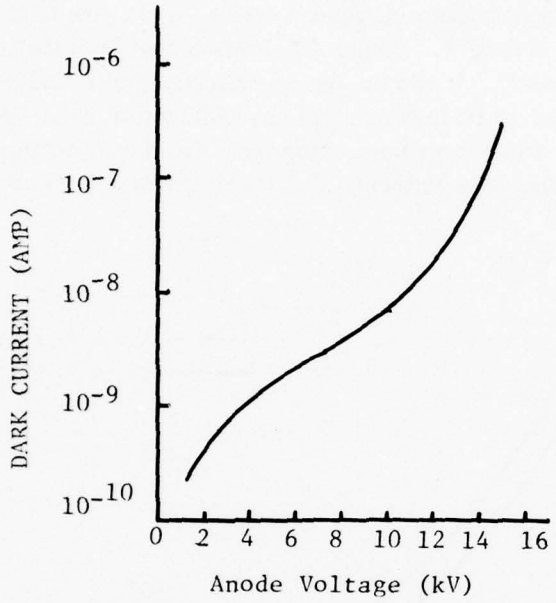

Figure 12. Dark current vs anode voltage. (Extended red multi-alkali photocathode) (Sensitivity: 235 Aμ lm^{-1}; d = 2.1 mm) (After J.A. Cochrane, et al, "Adv. in E. E. P., Vol 40A, P. 444).

5.5 kV/mm is believed to be due to the Schottky effect, which lowers the potential barrier at the surface. The observation of the sharp increase in Equivalent Background Input (EBI) is an indication of the surface nonuniformity, whose nature would be very interesting to be looked into. The sharp knee occurs before the onset of a visible emission point (bright spot). The dark current (see Figure 12) will vary according to the following relationship:[6]

$$I = I_o e^{C\sqrt{BE}}$$

where I_o is the low field thermionic emission, C is a constant to take care of the permittivity of the photocathode, and B is the multiplier. On the other hand, the photocathode noise can be increased in the absence of an emission point due to the field-enhanced thermionic emission over the whole surface. The field strength (Em) which will give the equivalent background input (EBI) to a level of 0.2 μ lux (about 10^{-8} ft-cd: in comparison, overcast night sky is about 10^{-5} ft-cd) is given as the following:

---

[6] J. A. Cochrane and R. F. Thurmond, "Adv. in E.E.P.," Vol. 40A, p. 444 (1976).

$$Em = \left[162 \log_{10} \frac{0.25\ S}{10^{16}\ J_o}\right]^2 \text{ volt/cm}$$

where S is the cathode sensitivity in A-μlm^{-1} and J_o is the low-field thermionic emission current density in A-cm^{-2}. Figure 13 shows a few hypothetical conditions of various values of S and J_o. It can be argued correctly that a Cs-GaAs photocathode has no potential barrier to be lowered, and any conduction band electrons regardless of origins can escape into the vacuum. However, the above mentioned phenomenon does exist. The EBI increases suddenly at 3.1 kV/mm or 3.5 kV/mm in most of the wide-gap diodes.

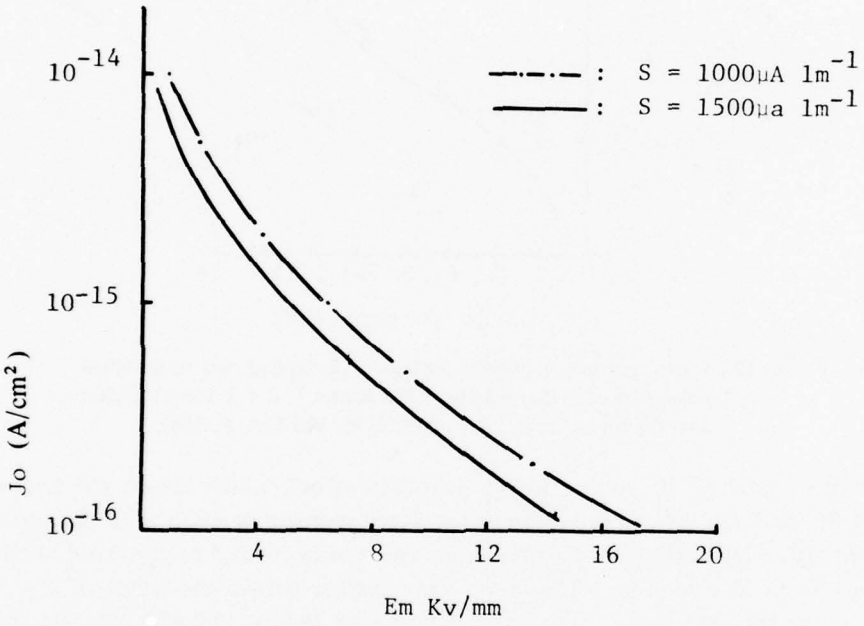

Figure 13. Em dependence on thermionic current density of a Photocathode for various sensitivities.

In some wide-gap diodes, the EBI curve (Figure 12) does not have a sharp knee even up to 4 kV/mm. It is plausible that the growth technique and/or the etching technique are such that a good surface was obtained. Note that the sharp knee occurs at 5.5 kV/mm in an extended S-20 photocathode (Figure 12). The size of a whisker which can cause the field enhancement can be as small as 1μm in diameter and 20μm in length.

It is interesting to know that loosened electrical contact metals and sharp indium points, which are formed inadvertently when two sections of a tube are pressure-sealed with In (Indium), cause a form of a field emission point – the emission point moves around as the tube is shaken and/or the emission points form a ring of bright glow around the edge of the tube.

2. **Microchannel Plate (MCP).** An MCP is made by various methods. One of them is fusing and drawing a bundle of clad glass fibers which is then chemically etched to make the cores hollow. The center-to-center distance between the adjacent channels is about 12 to 15μm, and the thickness of the wall is about 2 to 3μm. A smaller center-to-center distance in an MCP improves the resolution. (Sometimes "persistence" effect used to occur. "Persistence" is a phenomenon where an I^2 tube has an unusually long decay time (order of minutes instead of less than a second) after a pulse of high flux of light. This problem is eliminated after a refinement in the chemical cleaning process is made.) During the "coring out" process (making the MCP hollow), a flaring of the channel can take place to increase the open-area ratio. After the chemical cleaning, the MCP is "scrubbed" in high vacuum by electron bombardment. "Scrubbing" is a process where an MCP is bombarded by electrons, either from an electron gun or an opaque photocathode which is illuminated with light, while there is a potential drop across it. This process removes impurities from the MCP glass and also lowers the secondary emission yield at the same time.

In a 3rd gen tube, ions are kept from reaching the photocathode by means of an Al_2O_3 layer at the input of the MCP. The MCP is slanted 5°, with respect to the normal direction of the photocathode. "Slanting" facilitates collision of electrons with the MCP walls for multiplication. The effect of an Al_2O_3 can be seen in a pulse-height measurement as shown in Figure 14.[7]

To improve the first secondary emission yield, δ (this will be covered in detail later) of the MCP various secondary emission materials have been used. Table 3[8] shows that the gain of various materials is 3 to 4.5 times better than an uncoated and uncleaned MCP.

[7] H. Pollehn, *et al.*, "Adv. in E.E.P.," Vol. 40A, p. 21 (1976).

[8] H. Pollehn, *et al.*, "*Adv. in E.E.P.*," Vol. 40A, p. 23,(1976).

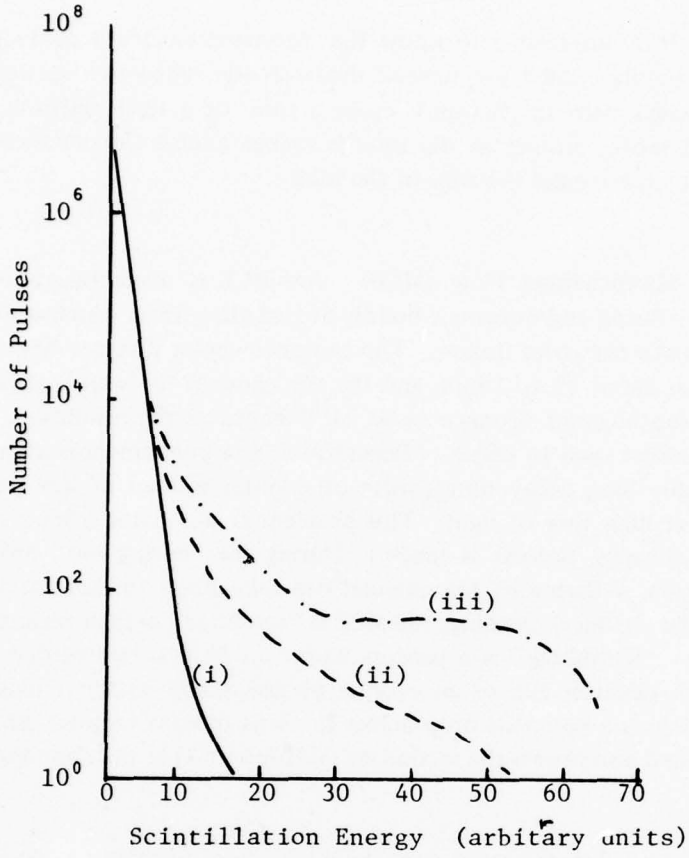

Figure 14. Pulse height distributions of wafer intensifiers: (i) Measured with an ultraviolet sensitive cathode in a facuum system; (ii) Measured in tube, input to MCP covered with Al_2O_3 film; (iii) Measured in the tube without Al_2O_3. (From H. Pollehn, et al, "Adv. in E.E.P.," Vol 40A, P. 23 (1976))

The glass wall of the MCP which is made of silica is made conductive by initially incorporating lead oxide and bismuth oxide and later partially reduced to lead (Pb) and bismuth (Bi) by heating it in hydrogen.[9] Potassium and carbon are concentrated on the surface. Potassium (K) has a great influence on the secondary emission yield (δ) of the glass.[10] The higher the potassium concentration is, the higher the secondary yield is. The δ of the glass wall of the MCP is also dependent upon the absorption or desorption of hydrogen, For example, exposure of the MCP to 1 torr of hydrogen for 1 hour at room temperature increased the yield by 8%.[11]

[9] G. E. Hill, "Adv. in E.E.P.," Vol. 40A, p. 153 (1976).

[10] *Ibid.*

[11] *Ibid.*

Table 3. Gain Increase of MCP with Secondary Emission Materials

Material	N_{FG}*	Gain (%)	Remarks
CsI	1.15	400	Very reproducible. No bake over 300°C. Stable under air bake at 250°C and light scrubbing.
KBr	1.15	450	No bake over 300°C.
MgF_2	1.30	300	Very unreproducible. δ_1 decreased by air bake.
MgO	1.35	300	Very independent on evaporation parameters. Stable for all tube processing and cleaning procedures.

* Best N_{FG} obtained.
Percentage increase compared to uncoated and uncleaned plate.
(after H. Pollehn, "Adv. in E.E.P.," Vol. 40A, p. 30 (1976).

Continuous electron bombardment of the glass wall depletes hydrogen and potassium, causing the degradation of the yield.[12] The secondary emission yield is also a function of the input electron energy. The yield increases at first as the primary energy does, but as the energy is increased more, the secondary electrons are generated at a greater depth. There is a higher probability for them to lose energy by inelastic scattering on the way to the surface and to fail to escape. The electrons also may not have sufficient energy to overcome the potential barrier at the surface even if they reach the surface.

The δ is also a function of the incident angle.[13] As the incident angle increases, the distance normal to the surface decreases, thus facilitating a higher yield (shorter escape distance to the surface).

The MCP also traps various gas molecules which, on being ionized by electrons, travel backward and hit the photocathode causing permanent damage if the energy is high. As mentioned earlier, a layer of Al_2O_3 is designed to stop the ion bombardment. Other methods have been tried to stop the ions: angled electrostatic field,[14] a photoetching technique,[15] a chevron of two MCPs, and a curved-channel technique.

[12] A. Authinarayanan, *et al.*, "Adv. in E.E.P.," Vol. 40A, p. 170 (1976).

[13] G. E. Hill, "Adv. in E.E.P.," Vol. 40A, p. 153 (1976).

[14] J. G. Timothy, "Rev. Sci. Instrum.," *45*, 6 (1974).

[15] W. Baumgartner, *et al.*, "Adv. in E.E.P.," Vol. 33A, p. 125 (1972).

Currently, 3rd gen tubes are made with a 5° slant and a layer of Al_2O_3 at the input of MCP using straight MCPs.

It is interesting to note that when an MCP is operated in the charge saturation mode, where the number of electrons is so large that the space-charge reduces the electrostatic field,[16] the pulse-height distribution is peaked, and the relative variance drops to 0.1. The lowest measured gain noise figure was 1.06.

Figure 15[17] shows that as the gain is increased, the pulse-height distribution narrows further.

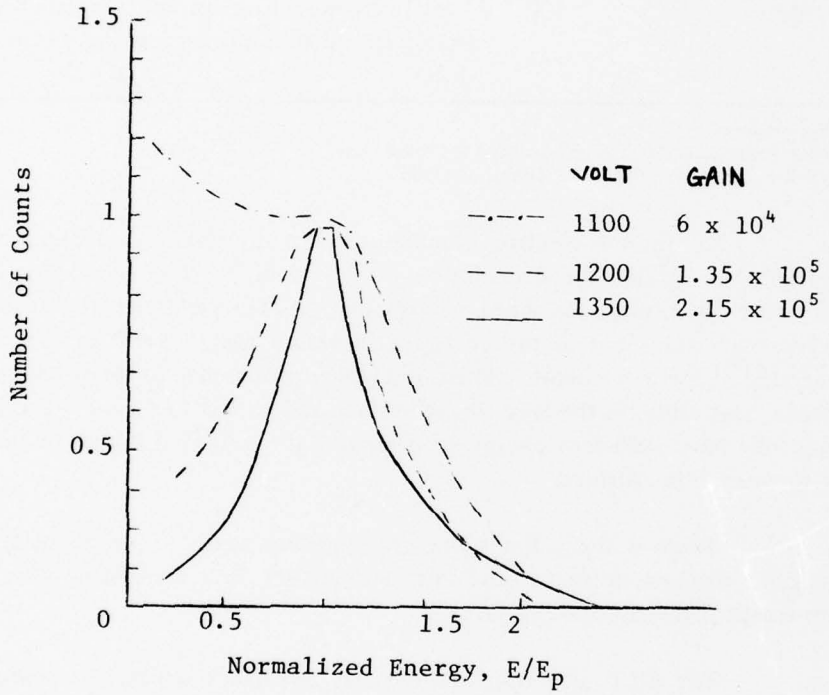

Figure 15. Pulse height distributions for MCP's.
(After H. Pollehn, et al, "Adv. in E.E.P.," Vol 40A, P. 25 (1976)).

Figure 16[18] shows the decrease in the relative variance as the MCP approaches saturation.

---

[16] C. Loty, "Acta Electron.," *14*, 107 (1971).

[17] H. Pollehn, *et al.*, "Adv. in E.E.P.," Vol. 40A, p. 21 (1976).

[18] J. P. Boutot, *et al.*, "Adv. in E.E.P.," Vol. 40A, p. 105 (1976).

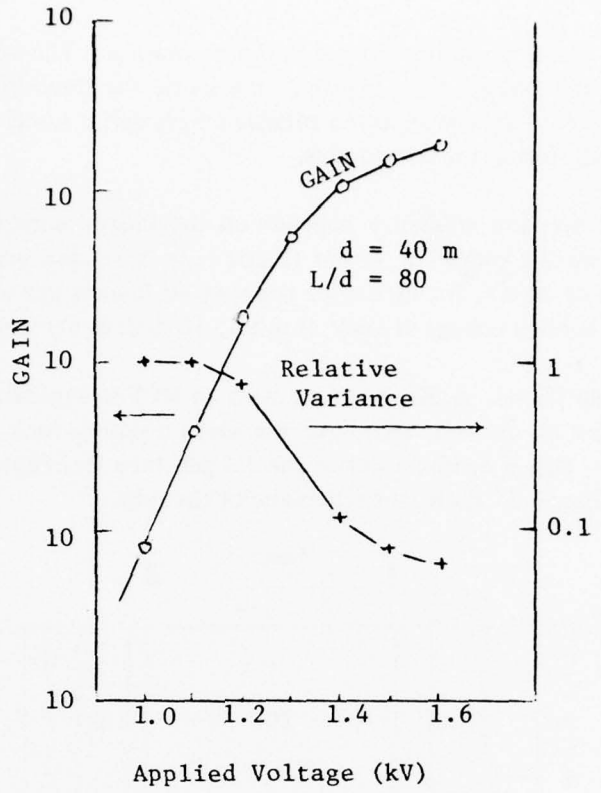

Figure 16. Gain and relative variance vs applied voltage.
(After J.P. Boutot, et al, "Adv. in E.E.P.," Vol. 40A, P. 105 (1976))

3. **Phosphor Screen.** A phosphor screen is made by various methods such as: settling, electrostatic, evaporation, and spraying. The noise of the screen depends upon the method used to make the screen. In a series of experiments, Beesley[19] found that the settled screen is about 2.7 times "noisier" than the electrostatically precipitated screen. The latter is found to be about 40% more efficient than the former.

The size of the phosphor particle affects the resolution and efficiency. The resolution is inversely proportional to the size. The smaller the particle size, the better the resolution becomes for a given thickness of the phosphor layer. But the efficiency goes down with particle size. A screen with larger size particles has higher efficiency than that with smaller size particles. The size of the screen particle used in an I^2 tube is a few microns. The thickness of the screen also must be optimized. A thick screen is desired to absorb all the electron energy and to maintain the uniform thickness – the relative variation can be made small in a thick screen.

[19] J. Beesley and D. J. Norman, "Adv. in E.E.P.," Vol. 22A, p. 551 (1966).

However, a thin screen is desired to get better resolution. The wider the scattered light path (from the phosphor particles) is, the worse the resolution becomes. This problem can be solved by means of an intagliated phosphor screen, where the phosphor is packed into slots in the fiber optics.

Conversion efficiency depends on the kinetic energy of the electrons when they land on the phosphor screen (P-20). In a 3rd gen wide-gap diode with a landing voltage of 20 kV, the efficiency is about 40 lumens per watt. In a 3rd gen MCP tube with a landing voltage of 6 kV, it is only 10 lumens per watt.

D. Wide-gap Diode. A 3rd gen tube with an MCP is expensive. To reduce the price per unit tube, an old tube technique was given a serious look again. It is called a wide-gap diode. It is a combination of the 1st gen tube technique and the 3rd gen tube technique. Figure 17 shows the schematic of the tube.

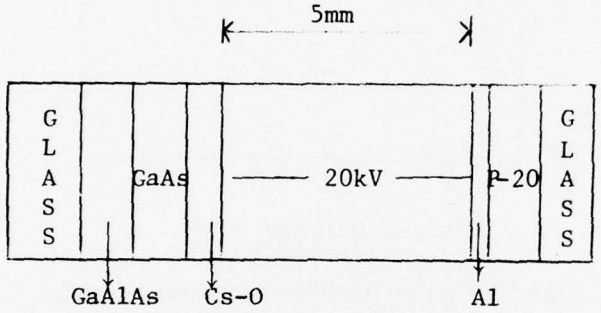

Figure 17. A wide-gap diode (not to scale).

The photocathode is made of GaAs with negative electron affinity, but the image intensification is obtained by bombarding the phosphor screen with high-energy electrons. The total gain of the tube is only on the order of 1000. In comparison, a typical 3rd gen tube has a gain of 10,000. A wide-gap diode should have a lower noise figure simply because it does not have an MCP (see Table 1). The wide-gap diode is being operated at a voltage of 20 kV. In some of the tubes measured, EBI has a sharp increase point at around 15 kV. Field emission of electrons or ions can increase the noise figure; however, it should not have an exponential distribution in the pulse height. (This will be explained later.) High-voltage operation of an earlier I^2 tube is known to increase the bright scintillations.

A 2nd gen tube has increased concentration of bright scintillations when the photocathode voltage is increased to about 1000 volts (this corresponds to 4000-5000 V/mm in a 2nd gen wafer tube). A similar phenomenon was observed in a 3rd gen MCP tube at about 1400 volts as discussed in the earlier section. (This corresponds to about 4.2 kV/MM.) (The development of a wide-gap diode was suspended because it lacked sufficient gain to be useful.)

IV. Statistics.

A. Noise Figure, N_F, and Gain Noise Figure, N_{FG}. N_F is defined by the following relationship:

$$N_F = \frac{S/N_{in}}{S/N_{out}}$$

where $S/N_{in} = \frac{1}{K} \; 2e\, i_t\, \Delta f$

$$S/N_{out} = \frac{DC_S - DC_B}{\sqrt{(AC_S)^2 - (AC_B)^2}}.$$

The terms will be explained in the following illustration of the experimental procedure: Input light of 1×10^{-5} footcandle forms a spot size of 0.2 mm in diameter on the photocathode and the photocathode current, i_t, is measured. The bandwidth, Δf, of the system and the I^2 tube is assumed to be 10 Hz (the correction factor, K, accounts for the deviation from it). The charge of an electron is e.

The DC_S and AC_S levels of the signal are measured. DC_B and AC_B levels of the background with no light input are also measured.

N_F is a number which represents a level of noisiness of an I^2 tube. N_F facilitates the ranking and the comparison among the I^2 tubes as to their relative performance, but N_F does not indicate why a tube has high or low performance.

The PHA attempts to explain the "whys" related to N_F. It complements N_F measurement by providing a detailed picture of the noise (scintillation or pulse height) spectra. One of the possible outputs of PHA is N_{FG}.

It was mentioned previously that N_{FG} is proportional to N_F,[20] but by no means should it be used in place of N_F if the constant is not known:

$$N_F = \frac{1}{\sqrt{D}} \; N_{FG}.$$

D is the detection probability of the electrons. It is the ratio of the number of scintillations out of the phosphor screen to the number of photoelectrons leaving the photocathode. D is obviously a function of many factors: the secondary yield

[20] H. Pollehn, "Analysis of Noise and Image Transfer Characteristics of Image Intensifier Tubes," NVL Report (1972).

δ of the MCP, the open-area ratio of the MCP input, the angle of the MCP with respect to flight of the electrons, and the chemical cleaning process of the MCP, among others. N_{FG} is calculated from the following relationship:

$$N_{FG} = \sqrt{\left(\frac{\sigma}{\langle E \rangle}\right)^2 + 1}$$

where σ is the standard deviation of the distribution and $\langle E \rangle$ is the average of the distribution.

The distribution of the scintillations (pulse height) is sometimes inherent to the multiplication system of an I^2 tube. An MCP normally has an exponential distribution gain:[21]

$$n_c = n_o e^{-Gi/Go}$$

where n_c is the number of pulses with gain of Gi, and Go is the average gain. The standard deviation is the same as the average, and $N_{FG} = 1.414$. For a Poisson distribution where $\sigma = \sqrt{\langle E \rangle}$:

$$N_{FG} = \sqrt{\frac{1}{\langle E \rangle} + 1}.$$

If the secondary emission yield per collision (bounce) is not constant, then the statistics assume a different look.

The δ of MgO is about 12 and the δ of the glass wall of the MCP is about 3. If the entrance of an MCP is coated with MgO, the first bounce yields a much higher number of electrons (12) than the bounce on the glass wall (3). If only two bounces are allowed, where the subscript designates the bounce, then the average gain per bounce and the variance of the gain are respectively δ_1 and δ_2 for the gain and σ_1^2 and σ_2^2 for the variance. The average gain for both is $\delta_s = \delta_1 \delta_2$, and the variance of the system is:

$$\sigma_s^2 = \delta_2^2 \sigma_1^2 + \delta_1 \sigma_2^2$$

$$= \delta_1^2 \delta_2^2 \left(\frac{\sigma_1^2}{\delta_1^2} + \frac{\sigma_2^2}{\delta_1 \delta_2^2}\right).$$

By iteration, the following relation is obtained for the k-bouncing system:

$$\sigma_{k\text{-}s}^2 = (\delta_1 \delta_2 \ldots \delta_k)^2 \left(\frac{\sigma_1^2}{\delta_1^2} + \frac{\sigma_2^2}{\delta_1 \delta_2^2} + \ldots \frac{\sigma_k^2}{\delta_1 \delta_2 \ldots \delta_k^2}\right).$$

[21] V. Chalmeton and P. Chevalier, "Acta Electron.," *14*, pp. 99 (1971).

If δ_1 is much larger than δ_i for $i \neq 1$ (12~13 for MgO), then SNR_k is simplified as:

$$SNR_k = \frac{\delta_k}{\sigma_k} = \frac{1}{\left(\frac{\sigma_1^2}{\delta_1^2} + \frac{\sigma_2^2}{\delta_1 \delta_2^2} + \ldots\right)^{1/2}} \cong \frac{\delta_1}{\sigma_1} .$$

For an exponential distribution,

$$\sigma_1 = \delta_1$$

therefore, $SNR_k = 1$.

For a Poisson distribution,

$$\sigma_1 = \sqrt{\delta_1}$$

therefore, $SNR_k = \sqrt{\delta_1}$

The signal-to-noise ratio of a Poisson distribution can be improved by having a larger δ_1.

The noise figure of a tube with a high initial yield δ_1 is defined as: [22]

$$N_{FG} = \sqrt{\frac{1}{\delta_1}\left(\frac{\sigma}{\langle E \rangle}\right)^2 + 1}.$$

B. Polya Distribution.[23] For the PHA, the input light level must be so low that there is virtually no probability of a coincident photoelectron event. The photoelectrons or thermal electrons are accelerated toward the MCP in an MCP tube with applied voltage of 900 V.

So far, a real I^2 tube has a distribution which falls between a Poisson[24] and an exponential distribution.[25] A single equation called Polya[26] (compound Poisson) distribution is used to describe the process with an adjustment parameter b.

Polya distribution is:

$$P(n,b) = \frac{\mu^n}{n!} (1 + b\mu)^{-\frac{n+1}{b}} \prod_{j=1}^{n-1} (1 + jb)$$

---

[22] H. Pollehn, "Analysis of Noise and Image Transfer Characteristics of Image Intensifier Tubes," NVL Report (1972).

[23] Photomultiplier Manual, RCA (1970).

[24] G. A. Morton, *et al.*, "Applied Physics Letters," Vol. 13, p. 356 (1968).

[25] L. A. Dietz, *et al.*, "Rev. Sci. Instrum.," *38*, p. 176 (1976).

[26] J. R. Prescott, "Nuclear Instrument Methods," Vol. 39, p. 173 (1966).

where P(n, b) is the probability of observing "n" secondary emissions for an arbitrary value of "b."

μ is the average value of the distribution.

b is the shape parameter of the distribution.

If b = 0, this becomes a Poisson distribution:

$$P(n, 0) = \frac{\mu^n e^{\mu}}{n!} .$$

If b = 1, this becomes an exponential distribution:

$$P(n, 1) = \mu^n (1 + \mu)^{-(n+1)}.$$

Figure 18 shows the shapes of various Polya distributions with different values of "b." Note that a Poisson distribution has a higher signal-to-noise ratio for a given mean value than that of an exponential distribution.

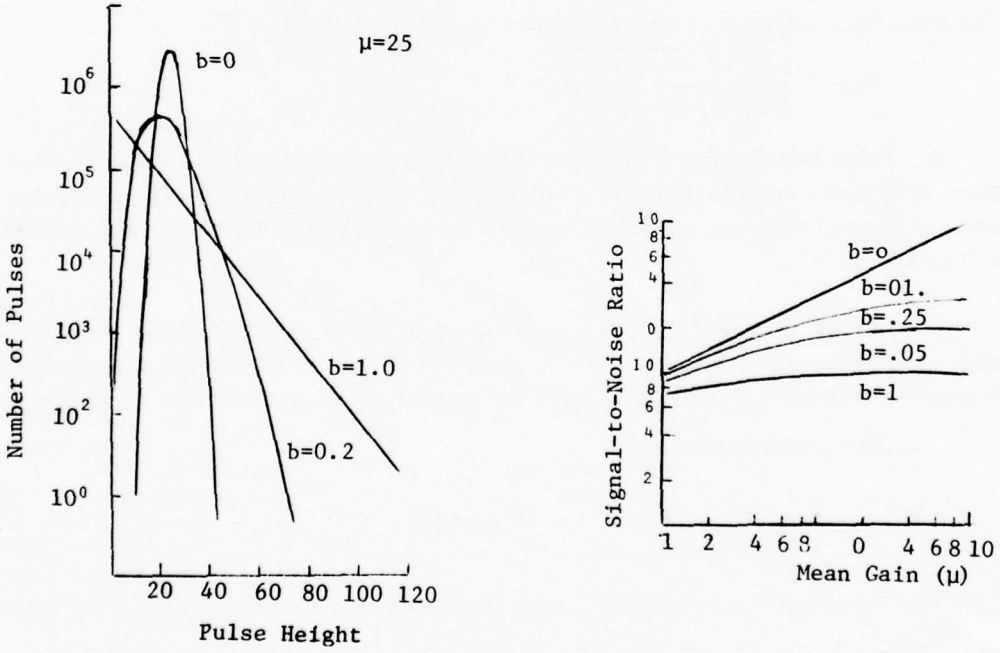

Figure 18. Polya distribution.

a. Various Values of "b." b. Signal-to-noise ratio.
(After *RCA Photomultiplier Manual*, p. 75 (1970), RCA, Solid State Division, Electro-Optics and Devices, Lancaster, PA. 17604).

C. **The Average Pulse Height and Its Variance**. The MCA plots the pulse-height distribution as the number of pulses per channel vs the channel number. Since the channel number is proportional to the pulse height (the number of photon contents per scintillation), the following relationship can be established (see Figure 19):

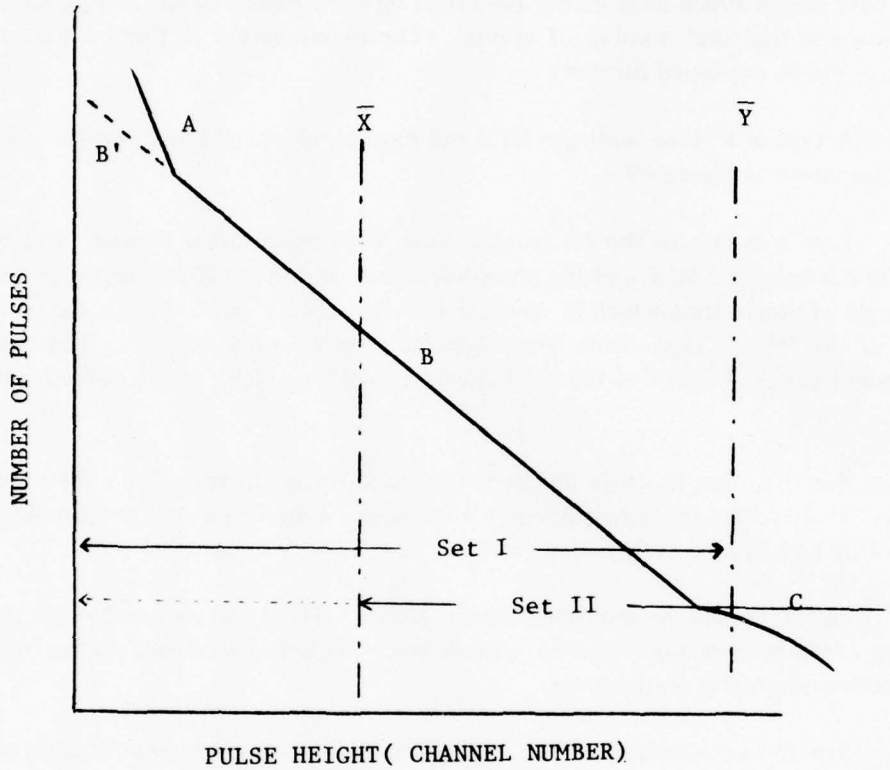

Figure 19. Number of pulses as a function of pulse height. (Pulse height distribution)

$$E = \frac{\int_0^\infty E\,N(E)\,dE}{\int_0^\infty N(E)\,dE}$$

$$N_i = \int_0^\infty N(E)\,dE$$

$$\sigma^2 = \frac{\int_0^\infty (E - \langle E\rangle)^2 N(E)\,dE}{\int_0^\infty N(E)\,dE} = \langle E^2\rangle - \langle E\rangle^2.$$

V. Data Acquisition.

A. General. Two sets of data are collected for PHA: Set I and Set II. Set I contains most of the output data for the experiment while neglecting a few higher energy data points which have hardly any effect on the outcome of the average energy evaluation and the total number of events. (The extrapolation method is used for this and it will be explained further.)

A typical I^2 tube with the MCP will have a pulse-height distribution similar to the one shown in Figure 19.

Part A is due to the electronics noise, PMT noise, other thermal electrons from the contacts, the MCP and the phosphor screen, and irregularly decaying portion of a single photoelectron which is counted as a low-energy noise due to the gating nature of the MCA. They come from the area after the photocathode. Therefore, they do not get the benefit of the total energy which is available to the cathode electrons.

Part B is due to single photoelectrons and single electrons from the photocathode. It describes the intensification process of a tube whether it is by multiplication or by high kinetic energy.

Part C is due to multiple-electron events. These are caused by the field emission – minor or major – and by positive ion bombardment. These are the bright scintillations observable on the screen.

For the convenience of the data analysis, the plot on Figure 19 is divided into two sets as mentioned earlier. Set I consists of the curve to the left of the line Y. Set II *looks* like a curve from the right of the line x, but actually Set II consists of the whole distribution. The scale ratio of Set I and Set II is 1:10 normally (this will be shown more explicitly later).

The generation rate of the data for Part C is much lower, a few orders of magnitude, than that of Part A and Part B. Three statistical parameters are desired to be obtained from the experiments: the total number of the population N_i, where the subscript i is the experimental run number; the average of the population $\langle E \rangle$; and the standard deviation of the population σ.

The effect of few counts in Part C will be examined in detail. The pulse-height distribution is assumed to be an exponetial function:

$$n_i = n_o e^{-\alpha i}$$

where n_i = number of counts in ith channel.

n_o = constant.

α = slope of the function.

i = channel number.

Table 4 summarizes various hypothetical situations. Basically, the distribution function spans from the 0th channel to the 200th channel, and there are 10 counts in the 220th channel. First, various numbers are calculated without the 220th channel counts. Then, the numbers are recalculated including the 220th channel counts.

Table 4. Effect of a Few High-Energy Pulses on $\langle E \rangle$ and σ*

Pulse Counts Up to Channel 200					Pulse Counts Including 10 Counts at Channel 200			
n_o	α	N_i	$\langle E \rangle$	σ	$\langle E' \rangle$	σ'	ΔE	$\Delta\sigma$
10,000	0.046	216,920	21.7	21.5	21.7	21.6%	0.05%	0.3%
1,000	0.034	28,985	29.0	28.2	29.1	28.4%	0.23%	1%
500	0.031	16,058	31.6	26.7	31.8	25.2%	0.44%	5.9%

* See text for explanation of terms.

It is obvious that few counts in the high-energy channels can be ignored in calculating N_i and $\langle E \rangle$, and, to a certain extent, the standard deviation, σ, if the total population is large. However, if the total population is small, the discrepancies in N_i and $\langle E \rangle$ are still negligible but not the discrepancy in σ.

Set I is used to find the average $\langle E \rangle$ and the total number of the population N_i and σ can be used to calculate N_{FG} if it is useful. But it should not be used out of context. $\langle E \rangle$ and N_i are used to rescale Set II. Set II, therefore, is the rescaled version of the output so that all the high-energy pulses which were not included in Set I are included while losing the low-energy resolution as mentioned above. The low generation rate of Part C is made up by the increased input photon flux.

B. Specific. The PMT voltage affects both the data collection rate and the output pulse height, other experimental conditions being the same. Since it is desirable to involve a fewer number of variables, NV&EOL attempts to use a constant PMT voltage for both Set I and Set II. When an unknown tube is to be examined, a rather high level of light, which insures a high rate of data generation, is used for the purpose of quick scanning of the data output.

An approximate facsimile of Set I (Figure 19) is obtained initially with a high amplifier gain. Without changing the PMT voltage, the amp gain is lowered and the light level is increased in order to obtain a facsimile of Set II (Figure 19). The amp gain and the PMT voltages are adjusted until no high energy pulse is lost in Set II while maintaining the facsimiles of Set I and Set II in Figure 19. This is a trial and error method in order to get two sets of workable output data with the variables confined to the light level, the amp gain, and the scanning time while keeping the PMT voltage constant. (This is not absolutely necessary if the discrepancy can be accounted for.) Part A serves as a reference for Set I and Part B for Set II. Of course, it is not absolutely necessary to have Part A as will be shown later, but its existence eliminates the uncertainty as to whether Part B is the result of the extrapolation of B or A.

The following relative conditions are expressed for Set I and Set II. (The actual conditions will be shown in a later section.) Assuming the PMT voltage is constant:

Set I
- Light Level: low (L_1)
- Amplifier Gain: high (G_1)
- Accumulation Time: short (T_1)

Set II
- Light Level: high (L_2)
- Amplifier Gain: low (G_2)
- Accumulation Time: long (T_2)

VI. Data Analysis.

A. Theory. The actual pulse-height distribution is reproduced in Figure 20. Note the absence of Part A on curve P from which the noise was subtracted. Curve M is obtained at the aperture setting 5 (the relative value of 3000), the PMT voltage 1600 volts, and the amplifier gain 200. The tube has a gain of 10,000, and the power-supply voltage was 2.7 volts. Curve N is obtained from curve M: after the curve is obtained, the input light is turned off and the MCA is operated in the subtraction mode for the same duration as that for curve M. Curves O and P have the same relationship as that between curves M and N. The only difference is that the light level for the M is 91 times higher than that for the O.

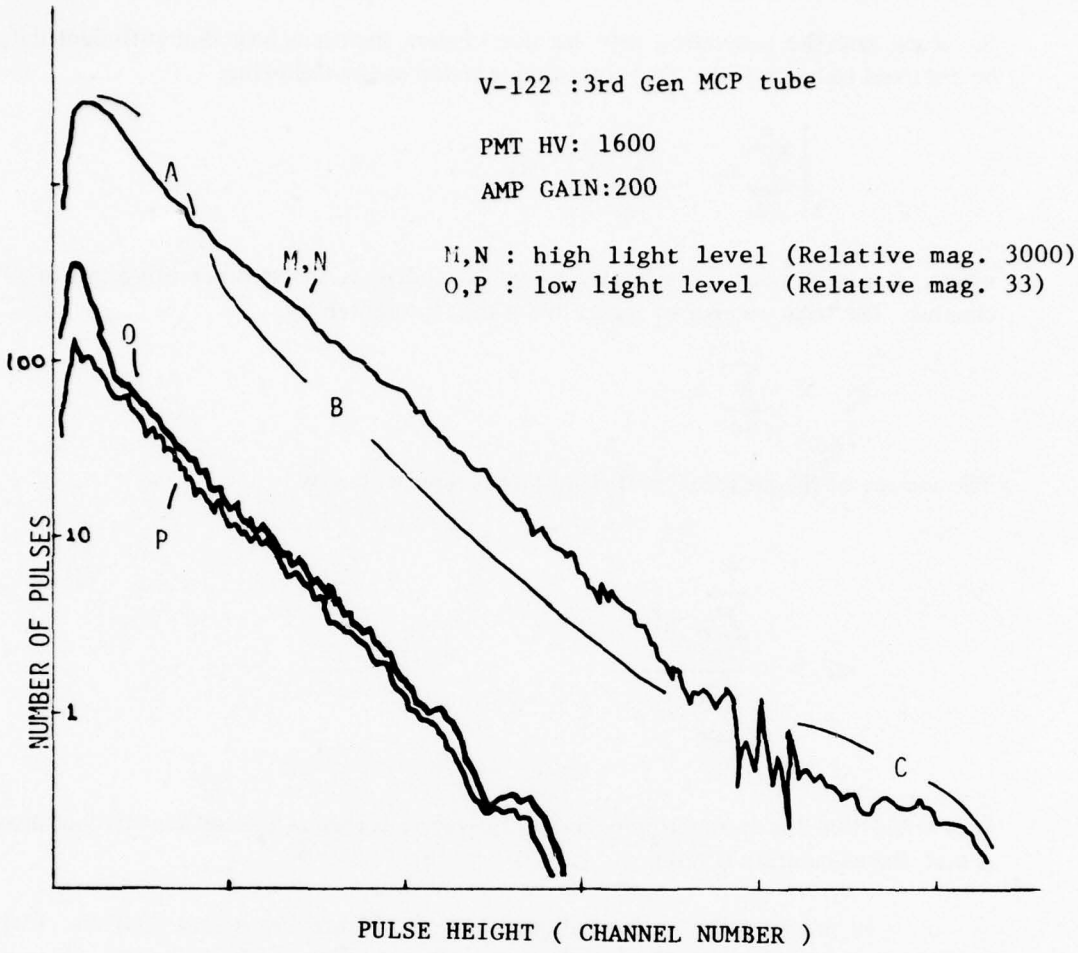

Figure 20. Effects of the noise subtraction at high and low light level.

When the input light level is high, it does not make any difference whether the noise is subtracted from the signal or not (see curve M and curve N in Figure 20). However, if the light level is low, the noise subtraction (curve P) gives an insight as to the justification of the extrapolation of Part B to get Part B′ in Figure 19.

Two things in Figure 20 are very important. First, the slopes of Part B of the curves M, N, O, and P are the same. This is an implicit justification of using a high light-level to obtain sufficient data rapidly. Second, the high-energy scintillations are not obvious in the O and P while they are quite noticeable in the M and N. If the slope of the high-energy scintillations is the same as that of the low-energy scintillations (Part B in Figure 19), then it is quite easy to create the data artificially. But if

the slope and the generation rate are not known, then it is best that sufficient data be obtained to begin with. This condition is stated as the following:

$$\left| \sum_{i=0}^{m} n_i - \sum_{j=0}^{n} n_j \right| < \epsilon$$

where m, n <N, m≠n for arbitrary ϵ and N, and n_i is the number of counts in ith channel. The total number of pulses in Set I is represented by:

$$N_j = \sum_{i=0}^{i} n_i$$

The average of the pulse-height distribution is represented by:

$$\langle E_1 \rangle = \frac{\sum_{i=0}^{j} n_i E_i}{\sum_{i=0}^{j} n_i}$$

It is noted that the summation is finite. However, as long as the sufficiency condition is met, the calculation is valid.

In practice, the extrapolation of Part B (Figure 19) is very difficult. First of all, one must identify and recognize where Part A ends and Part B starts. A common mistake is either to regard Part C as Part B or Part A as Part B. In the former case, the average energy is higher than it should be, resulting in a smaller standard deviation and a lower gain noise figure (N_{FG}). In the latter case, the average energy is lower than it should be, resulting in a larger standard deviation and a larger gain noise figure (N_{FG}).

Normally, one must go back and forth in the experimental setups between Set I and Set II in order to identify and optimize the test condition. If one misses the high-energy scintillations because of their infrequent occurrences, then the mistake mentioned above occurs. Two remedial methods are recommended:

1. In Set I, use the noise subtraction method (Figure 21) to identify the junction of Part A and Part B.

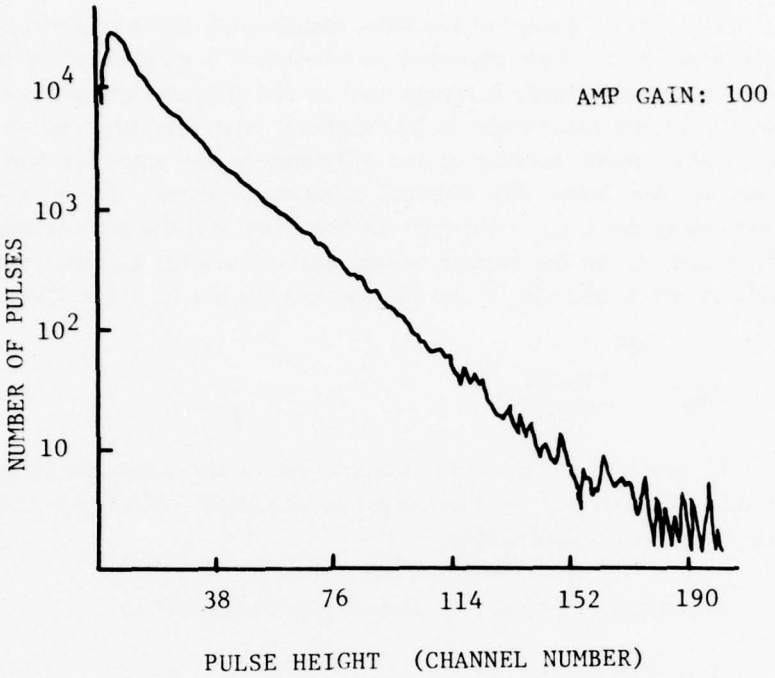

Figure 21. Set I from No. 40072.

2. In Set II, allow sufficient accumulation time with a low light level to make sure that none of the high-energy scintillations are clipped away.

Another difficulty arises because Part B is not always straight. This mistake comes about because of the assumption that Part B must be straight (even if one is forced to use the high amplifier gain) and must be extrapolated. The shape of Part B is a reflection of the secondary emission processes. For example, a 2nd gen tube will normally have a straight Part B (no MgO), but a 3rd gen tube with irregular MgO coating will have a zigzagged Part B. It definitely does not make sense to extrapolate the first zig out of a zigzag. If one remembers that the sole objective for the extrapolation is to eliminate the unuseful noise from the useful signal, the solution becomes clear. The noise-subtraction method (Figure 21) with a very low light level clearly indicates how the extrapolation must be done. In other words, it is possible to obtain the slope and the starting point of the extrapolation from a low light level noise subtraction method (of course, there can be exceptions). These problems become more confusing if one assumes that he must apply one method which worked for one kind of a tube to another without realizing that the other tube has a different kind of intensification process. Therefore, one should not take anything for granted.

The average energy of the pulse distribution, if the experimental conditions do not change, is the same regardless of whether it is represented in Set I or Set II. However, the average energy is represented by the different channel numbers in Set I and Set II. In the experiment to be described later, the difference in the channel numbers comes about because of the difference in the amplifier gain. The higher the gain is, the larger the channel number becomes: $E_1 = \alpha G_1$ where E_1 is the number in Set I, G_1 is the gain for Set I, and α is the proportionality constant. Let $\langle E_1 \rangle$ and G_1 be the average energy channel number and the amplifier gain respectively in Set I, and $\langle E_2 \rangle$ and G_2 the same in Set II. Then $\langle E_2 \rangle$ is related to $\langle E_1 \rangle$ by:

$$\langle E_2 \rangle = \frac{\langle E_1 \rangle G_2}{G_1}.$$

In order to facilitate the comparison of the noise-scintillation spectra of various tubes, the gain of the tubes must be equalized. This is done by dividing Set II by $\langle E_2 \rangle$ (X-axis normalization).

An arbitrary number (N_o) is chosen so that $N_i \alpha N_o$ or

$$N_i A_i = N_o \tag{1}$$

where A_i is a multiplier and N_i is the population of Set I. N_o has to be constant for the tubes to be compared with.

Next, it is desired to deduce which experimental parameters and measurement conditions affect the number of pulses (Y-axis) and the conversion ratio of the pulse energy into the channel number (X-axis) for each data set. The number of pulses per channel width increases with the input light level (L_1) and the accumulation time (T_1). For a given voltage of the PMT, the pulse height is proportional to the amplifier gain (G_1) when it is displayed on the MCA. Let the subscripts 1 and 2 designate Set I and Set II in A_i and N_i. Then, N_1 is represented as (N_1 is the measured number of population in Set I):

$$N_1 = D_o L_1 T_1 \times G_1 \tag{2}$$

where a constant D_o takes care of the relationship between the absolute input light level and the relative light level (L_1) used in the experiment and between the amplifier gain and the MCA channel number.

First, the distribution in Set I is normalized with respect to $\langle E_1 \rangle$ by dividing the X-axis value with $\langle E_1 \rangle$. Therefore:

$$N_1' = \frac{N_1}{\langle E_1 \rangle} \tag{3}$$

The normalized population N_1' is scaled according to the following:

$$N_o = A_1 N_1' = A_1 \frac{N_1}{\langle E_1 \rangle} \tag{4}$$

Similarly, the normalized (X-axis only yet) Set II is described as:

$$N_o = A_2 N_2' = \frac{A_2 D_o L_2 T_2 G_2}{\langle E_2 \rangle} \tag{5}$$

$$(N_2' = \frac{N_2}{\langle E_2 \rangle} \; ; \; N_2 = D_o L_2 T_2 G_2).$$

A_2 is the scaling number for Set II which must be found. Substituting D_o from Eqn. (2) into Eqn. (5) and rearranging:

$$A_2 = \frac{N_o}{N_2'} = \frac{N_o}{N_1} \frac{L_1 T_1 G_1}{L_2 T_2 G_2} \times \langle E_2 \rangle.$$

Since $\langle E_2 \rangle = \langle E_1 \rangle \frac{G_2}{G_1}$

$$A_2 = \frac{N_o}{N_1} \frac{L_1 T_1}{L_2 T_2} \langle E_1 \rangle \tag{6}$$

$$A_2 = \frac{N_o}{N_1'} \frac{L_1 T_1}{L_2 T_2} \tag{7}$$

The number of pulses per channel in Set II is multiplied by A_2.

In summary:

(1) The pulse height is normalized with respect to the average energy: the X-axis is divided by $\langle E_1 \rangle$:

$$N_1 = \frac{N_1}{\langle E_1 \rangle} .$$

(2) The input light condition of Set I must be equalized to that of Set II:

$$\frac{N_1}{\langle E_1 \rangle} \times \frac{L_2 T_2}{L_1 T_1} = N_1''.$$

(3) The scaled population N_1'' must be normalized to a constant number, N_o, for all the tubes to be compared: the Y-axis is scaled by $\frac{N_o}{N_1''}$.

As a result of the above argument *and* for an exponential distribution of $n_i = n_o e^{-\alpha E}$:

(1) After Step 1, $n_i' = n_o e^{-E}$, $N_1' \cong n_o$, and $\alpha = 1$.

(2) The scaling of the Y-axis corresponds to the scaling of the total population.

(3) After normalization and scaling, all the tubes with exponential distribution function will have the same function to describe Set I: $n: = N_o \exp(-E)$.

B. Experimental Results. Two image intensifier tubes were tested. The experimental conditions and the results are given and the analysis of the data is also followed through:

1. Tube #40072 – 2nd gen type with MCP experminetal conditions are:

Set I
Light Level (L_1): (Relative Unit 140)
Accumulation Time (T_1): 200 seconds
Amplifier Gain (G_1): 100
PMT Voltage: 1620 HV

Set II
Light Level (L_2): (Relative Unit 740)
Accumulation Time (T_2): 2000 seconds
Amplifier Gain (G_2): 10
PMT Voltage: 1620 HV

The number of pulses under B′, B, and C was counted, and the average of the pulse distribution is calculated in terms of the channel number in Set I. They are:

$$N_1 = 653{,}906.$$

$$\langle E_1 \rangle = 18.45.$$

Figure 21 shows the non-normalized Set I, and Figure 22 shows the non-normalized Set II.

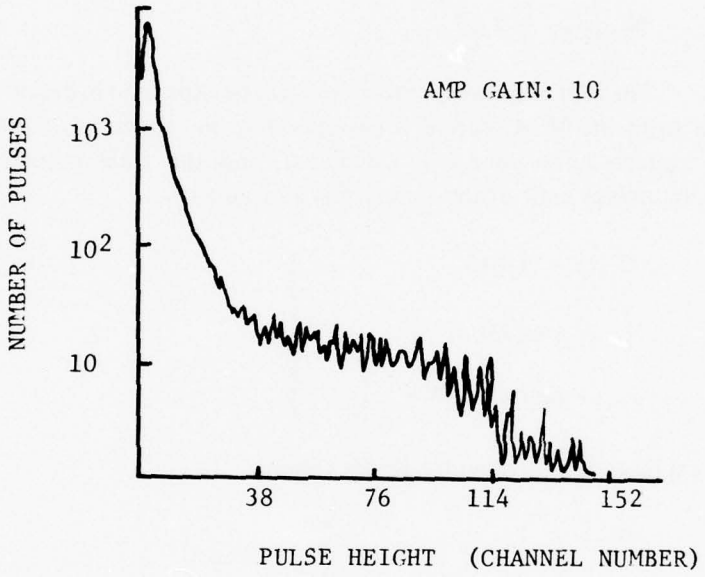

Figure 22. Set II from No. 40072.

The average in Set II is calculated in terms of the channel number:

$$\langle E_2 \rangle = \langle E_1 \rangle \times \frac{G_2}{G_1}$$

$$= 18.45 \times \frac{10}{100} = 1.845$$

The average pulse height in Set II is the channel number 1.845. The pulse height of Set II is divided by 1.845 (X-axis normalization).

Next, the number of pulses of the distribution is normalized to the total count of 10^7.

Using Eqn. (6):

$$A_2 = \frac{N_o}{N_1}\,\frac{L_i T_1}{L_2 T_2}\,E_1 = \frac{10^7}{653{,}906} \times \frac{140 \times 200}{740 \times 2{,}000} \times 18.45 = 5.34 .$$

Therefore, the vertical axis of Set II is scaled up by a factor of 5.34 (y-axis normalization). The gain noise figures of the normalized Set I and Set II are:

$$N_{(FG-1)} = 1.41$$

$$N_{(FG-2)} = 1.67.$$

The aforementioned procedure will be explained in detail. After Figure 21 is obtained from the MCA, Part B is extrapolated, the function of the curve is calculated, the average pulse energy is calculated, and the total population is counted (the upper and lower limit of the function is indicated):

$$\left.\begin{aligned} \langle E_1 \rangle &= 18.45 \\ N_1 &= 643{,}450 \\ n_1 &= 34875e^{-0.0542E}\Big|_0^{173} \end{aligned}\right\} \qquad \text{(G1)}$$

Next, the x-axis scale is divided by 18.45. Then,

$$\left.\begin{aligned} \langle E_1' \rangle &= 1 \\ N_1' &\cong 34.875 \\ n_1' &= 34875e^{-E}\Big|_0^{10.46} \end{aligned}\right\} \qquad \text{(G2)}$$

As expected, the exponential function behaves very nicely. Now, Set II is normaiized: the x-axis scale is divided by 1.845. Two exponential functions are fitted and their lower and upper limits are noted:

$$\left.\begin{aligned} n_2' &= 1871e^{-0.2511E}\Big|_{10.46}^{26.1} \\ n_3' &= 31.7e^{-0.0093E}\Big|_{26.1}^{71.3} \end{aligned}\right\} \qquad \text{(G3)}$$

The number (N_1') and the equation (n_1') in (G2) are scaled by $\frac{L_2 T_2}{L_1 T_1}$:

$$\frac{L_2 T_2}{L_1 T_1} = \frac{740 \times 2000}{140 \times 200} = 52.86$$

$$\left.\begin{aligned} N_1'' &= N_1' \times 52.86 \cong 1.843 \times 10^6 \\ n_1'' &= 1.843 \times 10^6 e^{-E} \Big|_0^{10.46} \end{aligned}\right\} \quad \text{(G4)}$$

The equations (n_1'', n_2', n_3') and the number (N_1'') are used to calculate N_{FG} of Set II.

$$N_{FG\text{-}2} = 1.67.$$

Use of the normalized function n_1'' with the functions n_2' and n_3' was necessary because the MCA used in the experiment showed unreliability in the lower channels: the lower channel portion of Set II is replaced with n_1''. Finally, for the pictorial representation, the Y-axis in (G3) and (G4) is scaled by A_2 (5.34).

Figure 23 shows the scintillation spectra of Tube #40072 rescaled and normalized.

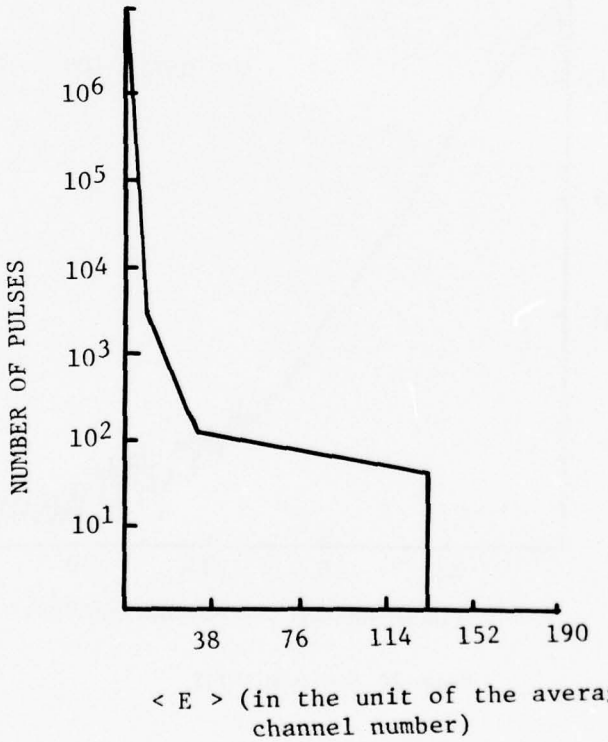

Figure 23. Normalized Set II from No. 40072.

2. Tube V-122 – 3rd gen type with MCP experimental conditions:

Set I
Light Level: 3000 (relative unit)
Accumulation Time: 30 seconds
Amplifier Gain: 100
PMT Voltage: 1620 HV

Set II
Light Level: 26000 (relative unit)
Accumulation Time: 200 seconds
Amplifier Gain: 10
PMT Voltage: 1620 HV

Figure 24 shows Set I, and Figure 25 shows Set II. Notice that in Figure 24 there is no Part "A" as in Figure 26. (The only difference between the two is the amplifier setting.) This becomes obvious when the amplifier gain is increased from 100 to 200 (Figure 26). Now, one sees Parts A, B, and C.

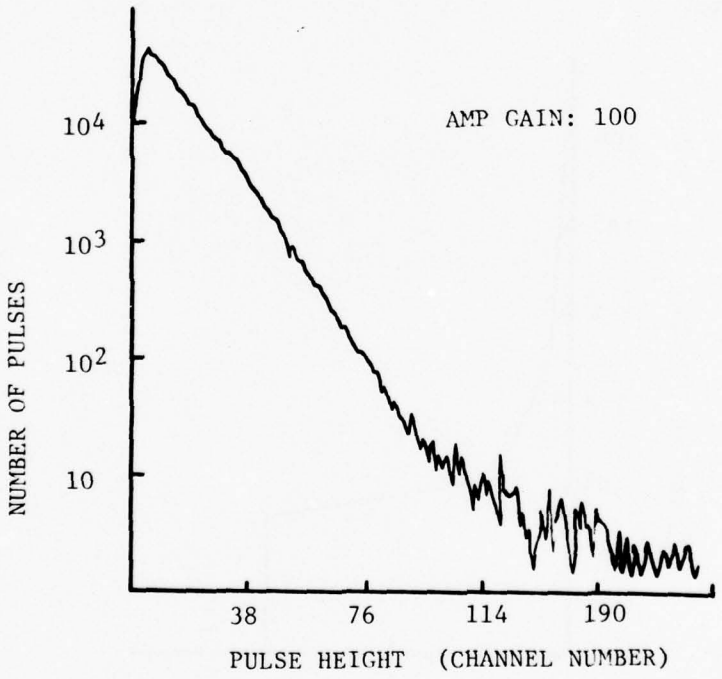

Figure 24. Set I from V-122.

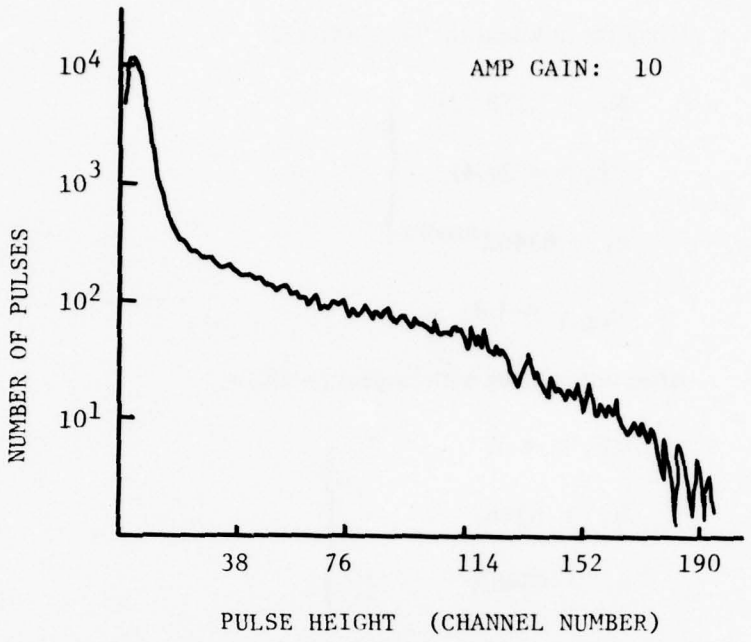

Figure 25. Set II from Tube V-122.

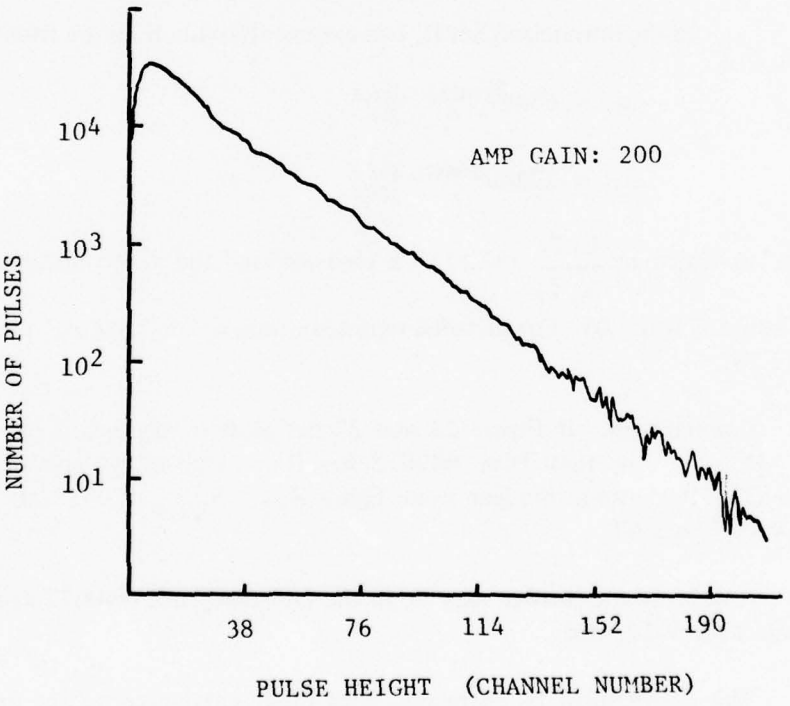

Figure 26. Set I from V-122 (3rd Gen Tube).

Using the notation for Tube #40072:

$$\left.\begin{aligned} N_1 &= 1{,}358{,}721 \\ \langle E_1 \rangle &= 21.41 \\ n_1 &= 63462^{-0.0467\,E} \end{aligned}\right\} \qquad (1)$$

$$N_{FG-1} = 1.41$$

After normalizing with respect to $\langle E_1 \rangle$:

$$\left.\begin{aligned} \langle E_1' \rangle &= 1 \\ N_1' &= 63462 \\ n_1' &= 63462e^{-E} \Big|_{0}^{11} \end{aligned}\right\} \qquad (2)$$

It should be noted now that both tubes show an identical slope, and the only difference is the population (check n_1' of Tube #40072 and Tube V-122).

In the normalized Set II, two exponential functions are fitted:

$$n_2' = 654e^{-0.0425E} \Big|_{11}^{56.5}$$

$$n_3' = 2230e^{-0.0682E} \Big|_{56.5}^{98.4}$$

After n_1' is scaled by $\frac{L_2 T_2}{L_1 T_1}$ (57.8), it is used with n_2' and n_3' to calculate N_{FG-2}. In this instance, it is 2.05. For pictorial representation, n_1', n_2' and n_3' are multiplied by A_2 (2.73).

C. Comparisons. If Figure 23 and 27 are plotted together, Figure 28 is obtained. It is obvious that Tube #40072 has fewer high-energy scintillations than Tube V-122. It shows in the gain noise figure N_{FG}. N_{FG-1} of V-122 is 2.05 while that of #40072 is 1.67.

A part of the answer may lie in the fact that Tube #40072 does not have MgO while Tube V-122 does.

The results must be correlated with other parameters of the tube and the fabrication technique.

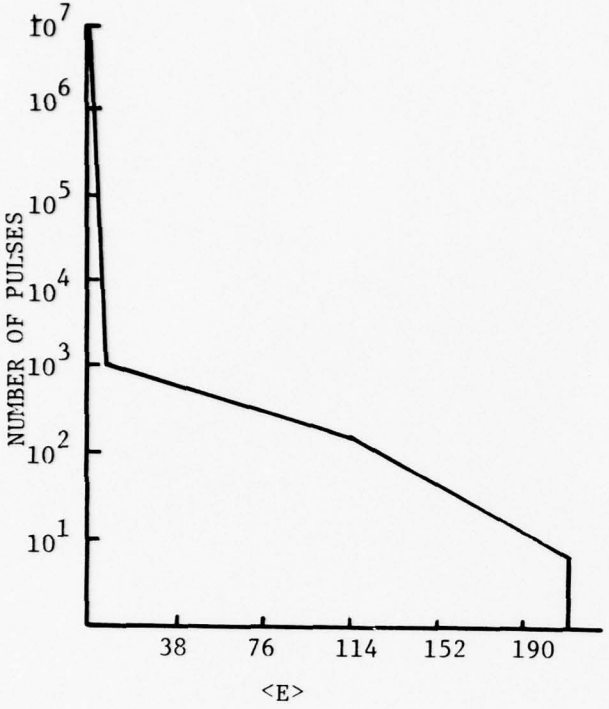

Figure 27. Normalized Set II of V-122.

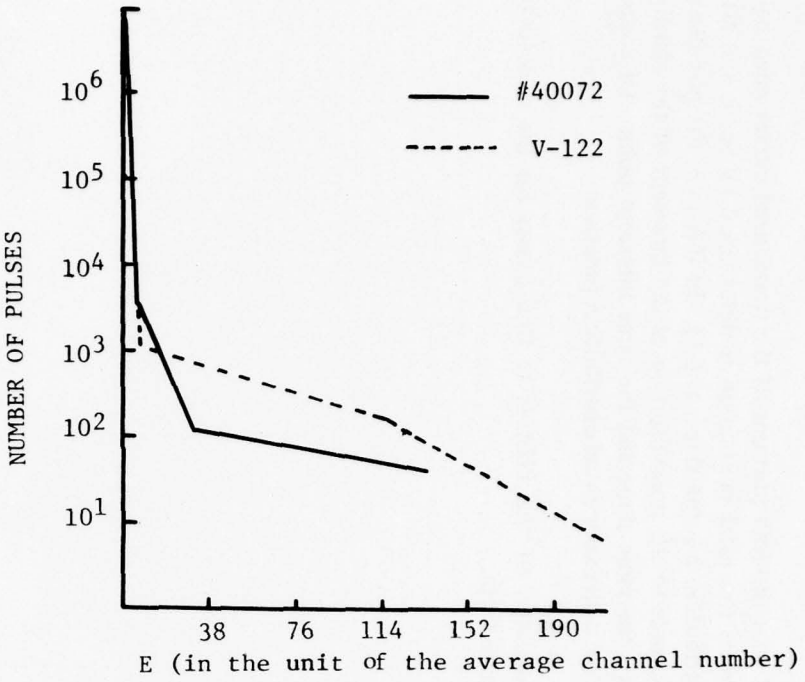

Figure 28. Normalized Set II from V-122 and No. 40072.

It is also noted that the first portions of the normalized curves must coincide with each other because the total population is determined by Set I, and after the normalization the distribution has the slope of (-1). In this case, the population normalization (A_2) corresponds to the normalization of the intercept of the distribution curve and the Y-axis: the same slope and the same intercept point. Of course, this is true only for the tubes with exponential distribution function.

The ultimate objective of the PHA is to find causes for the undesirable scintillations and to eliminate them.

BIBLIOGRAPHY

Authinarayanan, A., *et al.*, "Adv. in E.E.P." Vol. 40A (1976).

Baumgartner, W., *et al.*, "Adv in E.E.P." Vol. 33A (1972).

Beesley, J. and Norman, D. J., "Adv. in E.E.P." Vol. 22A (1966).

Bell, R. L., *Negative Electron Affinity Devices.* Clarendon Press, Oxford (1973).

Boutot, J. P., *et al.*, "Adv. in E.E.P." Vol. 40A (1976).

Chalmeton, V. and Chevalier, P., "Acta Electron." *14* (1971).

Cochrane, J. A. and Thurmond, R. F., "Adv. in E.E.P." Vol 40A (1976).

Dietz, L. A., *et al.*, "Rev. Sci. Instrum." *38* (1976).

Hill, G. E., "Adv. in E.E.P." Vol. 40A (1976).

Loty, C. "Acta Electron," *14* (1971).

McGee, J. D., Airey, R. W., and Aslam, M. "Adv. in E.E.P." Vol. 22 (1966).

Morton, G. A., *et al., "Applied Physics Letters," Vol. 13 (1968).*

Photomultiplier Manual. RCA (1970).

Pollehn, H. "Analysis of Noise and Image Transfer Characteristics of Image Intensifier Tubes." NVL Report (1972).

Pollehn, H., *et al.*, "Adv. in E.E.P." Vol. 40A (1976).

Prescott, J. R., "Nuclear Instrument Methods." Vol. 39 (1966).

Timothy, J. G., "Rev. Sci. Instrum." *45* (1974).

APPENDIX A

Schematic Diagram of Pulse Integration Mode

Pulse Integration Mode Schematic Diagram
(Configuration by Raymond J. Stefanik)

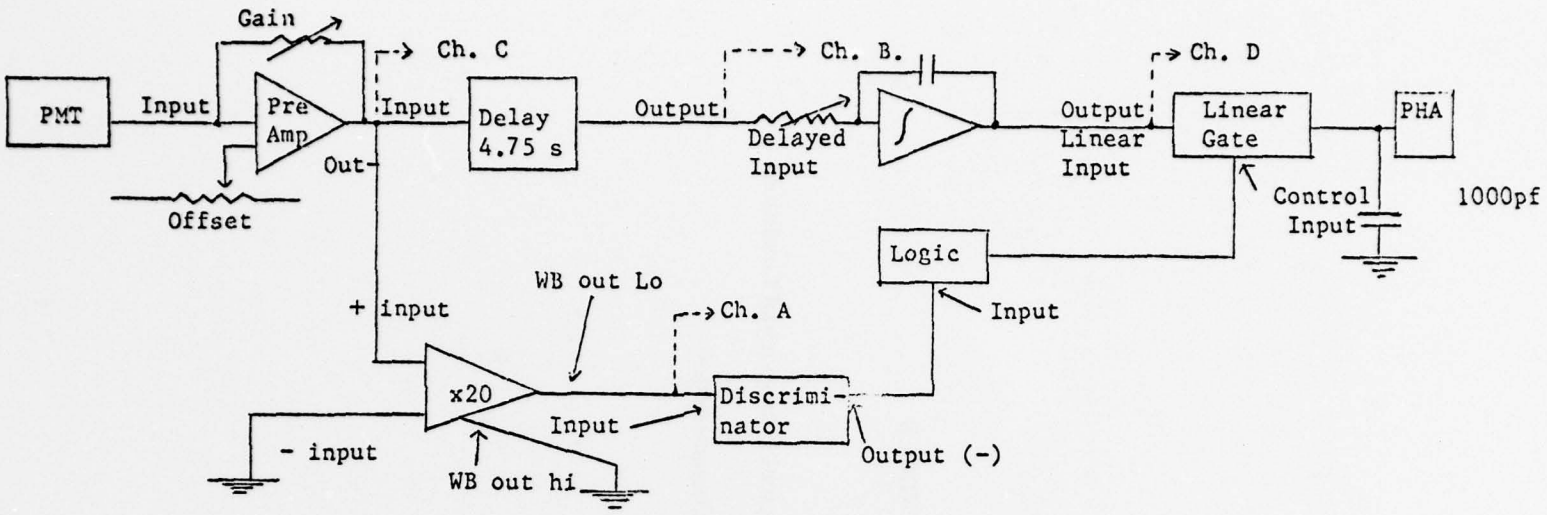

Equipment	MFR	Model	Serial	I.D. #	Settings
PMT	–	–	–	–	2 kV Max
Preamp	Homemade	–	–	–	In-, Out-
Delay	Tennelec	TC 215	207	12258-076	4.75 s
and Logic	Homemade	–	–	–	–
Linear Gate	Tennelec	TC 301	81	3706-076	Polarity +, Term 2K
X 20	Ectron	751 EK	8401	21531-076	Gain x 20
Discriminator	Tennelec	TC 405	24	11879-076	DC Level Detector
MCA	Northern	NS 170	–	6838	High Level, DC, Active

APPENDIX B

Oscilloscope Traces for Different Experimental Conditions and Tube Characteristics

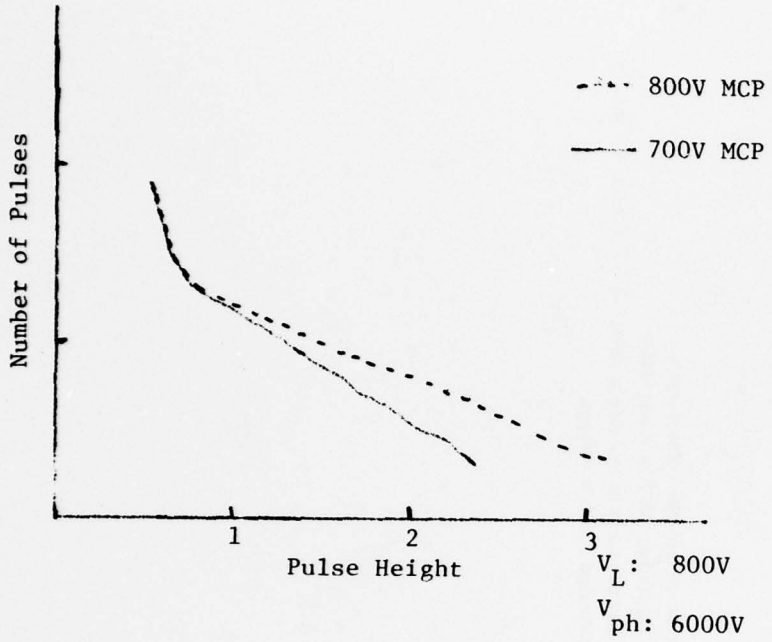

Figure B1. Variation on MCP voltage. (2nd Gen Tube: MCP without Mg0) Note that only parts "B" and "C" are affected by the increased MCP voltage.

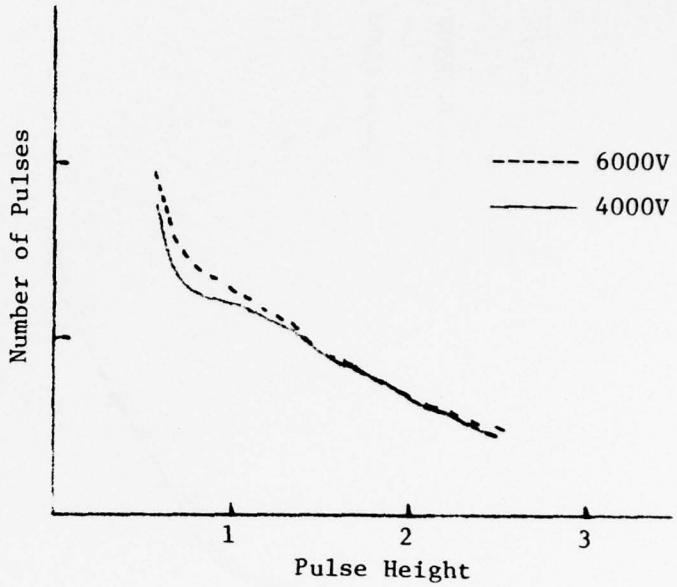

Figure B2. Variation on screen voltage only. (2nd Gen Tube: MCP without Mg0) Note that only parts "A" and "B" are affected by the increased screen voltage.

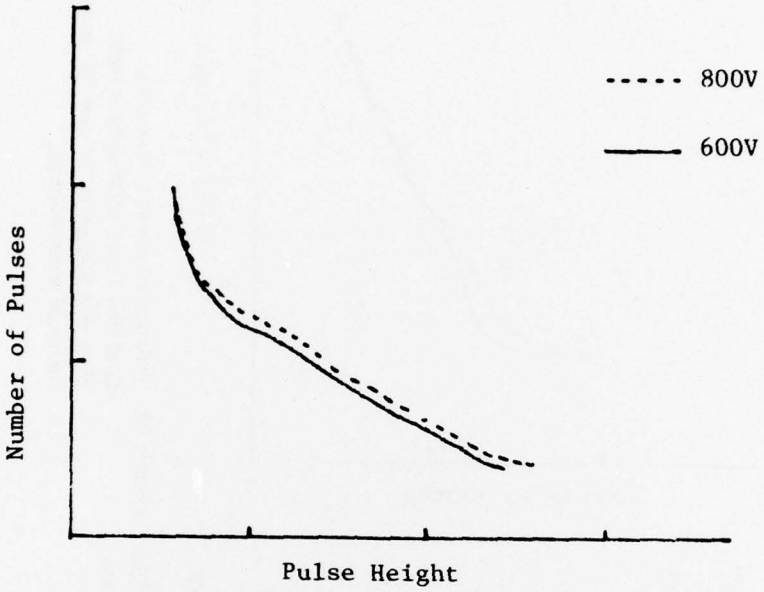

Figure B3. *Variation on cathode voltages only.*
(2nd Gen Tube: MCP without MgO)
Note that the unform increase in parts "A", "B" and "C" due to the increased cathode voltage.

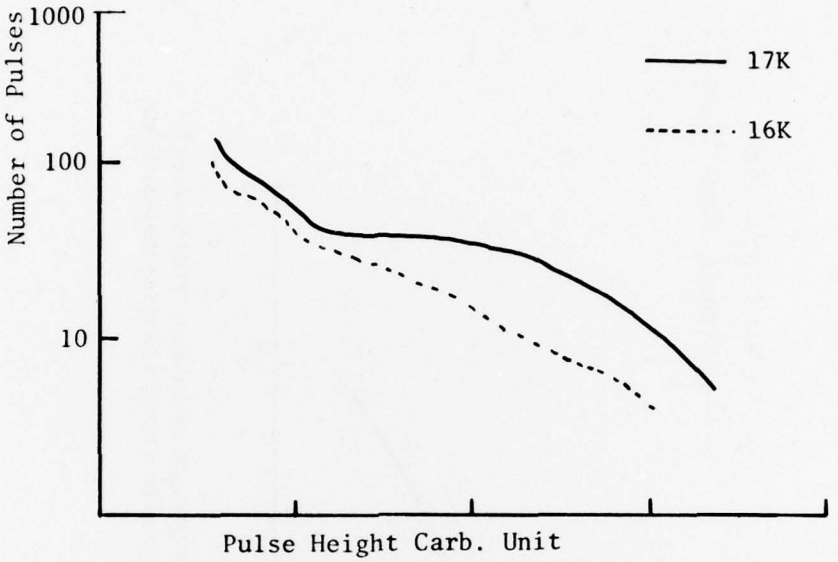

Figure B4. "Field Emission" in a wide gap diode (CB-001) at 17 Kv. It is not obvious at 16 Kv.

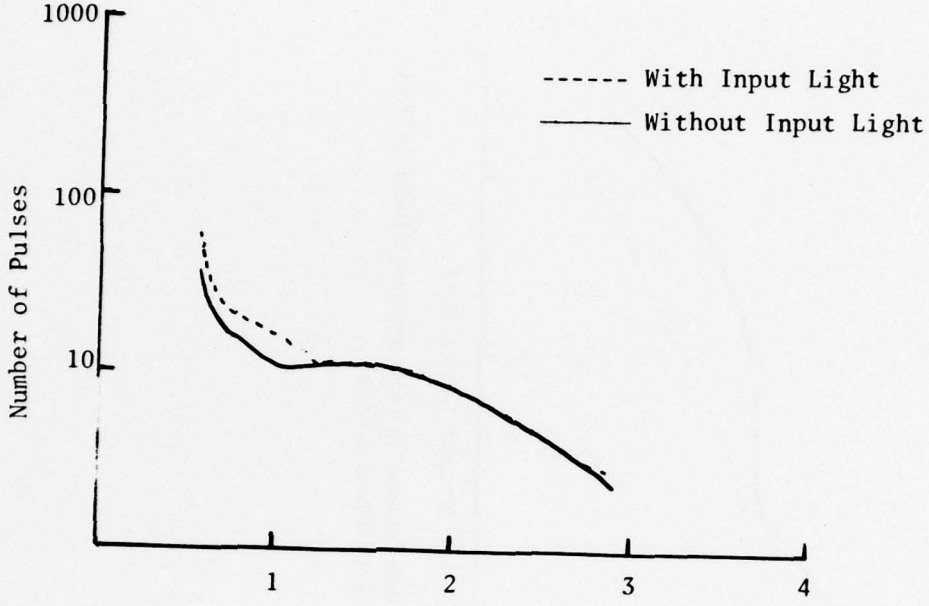

Figure B5. Effect of input light to the pulse height when there is "Field Emission." The population of high energy pulses is hardly affected by the input light.

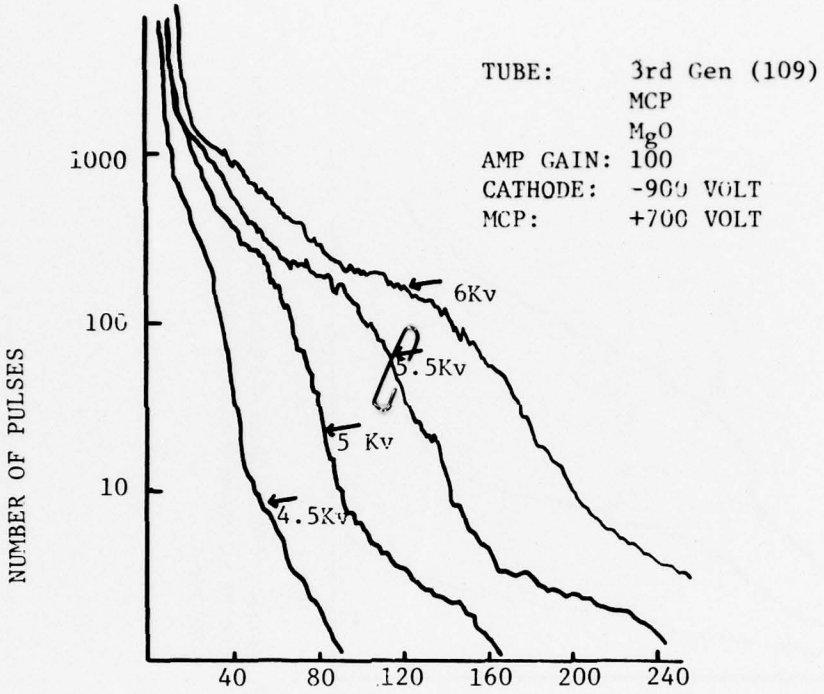

Figure B6. Variation of screen voltages only, in a low noise 3rd gen tube. Note the overall increase in the signal.

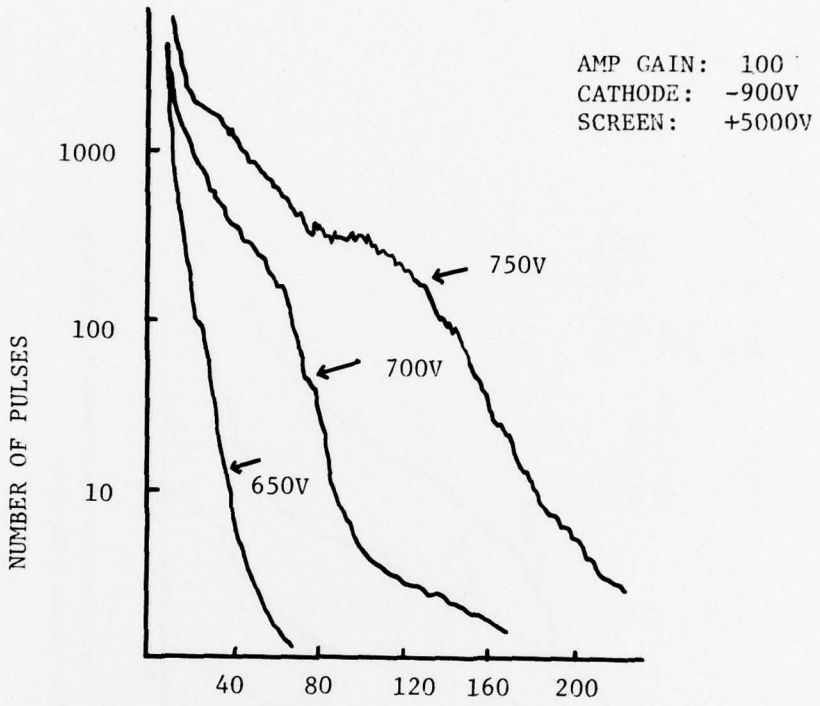

Figure B7. Variation of MCP voltages of a good, low noise 3rd gen tube. Note the appearance of a bulging hump, which reflects the scintillations.

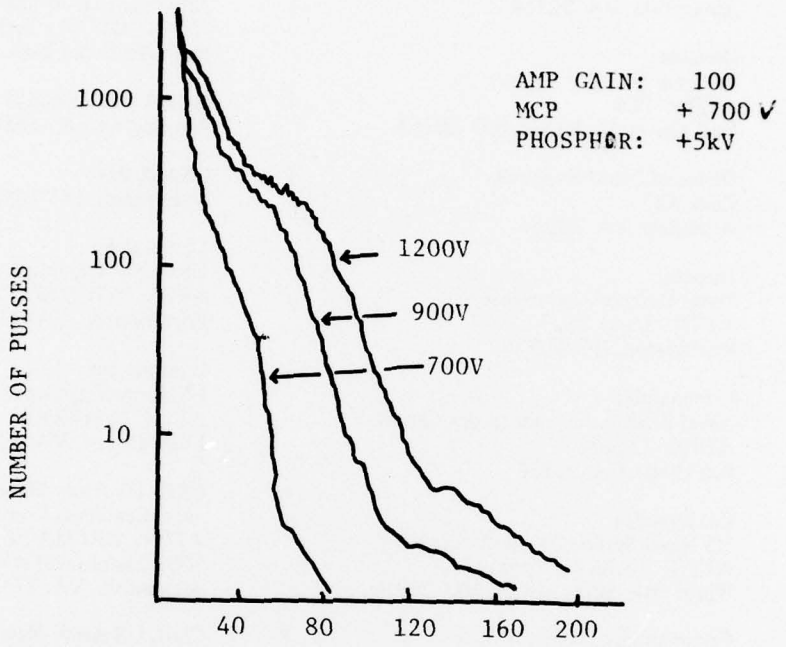

Figure B8. Variation of cathode voltages of low noise 3rd gen tube.

DISTRIBUTION FOR NV&EOL REPORT DELNV-TR-0006

No. Copies	Addressee
12	Defense Documentation Center ATTN: DDC-TCA Cameron Station (Bldg 5) Alexandria, VA 22314
1	Director National Security Agency ATTN: TDL Fort George G. Meade, MD 20755
1	Office of Naval Research Code 427 Arlington, VA 22217
1	Director Naval Research Laboratory ATTN: Code 2627 Washington, DC 20375
1	Commander Naval Electronics Laboratory Center ATTN: Library San Diego, CA 92152
1	Commander US Naval Surface Weapons Center ATTN: Technical Library White Oak, Silver Spring, MD 20910
1	Commandant, Marine Corps HQ, US Marine Corps ATTN: Code LMC Washington, DC 20380
1	HQ, US Marine Corps ATTN: Code INTS Washington, DC 20380
1	Command, Control & Communications Division Development Center Marine Corps Development and Educ Comd Quantico, VA 22134
1	HQ ESD (XRRI) L. G. Hanscom Field Bedford, MA 01730
2	Air Force Avionics Laboratory ATTN: AFAL/TSR, STINFO Wright-Patterson AFB, OH 45433
1	AFSPCOMMCEN/SUR San Antonio, TX 78243
1	Armament Development & Test Ctr ATTN: DLOSL, Tech Library Eglin Air Force Base, FL 32542
1	HQDA (DACE-CMS) Washington, DC 20310
1	OSASS-RD Washington, DC 20310
1	Commander US Army Training & Doctrine Cmd ATTN: ATCD-SI Fort Monroe, VA 23651
1	Commander US Army Training & Doctrine Cmd ATTN: ATCDOCI Fort Monroe, VA 23651
1	CRD, US Army Materiel Development and Readiness Command ATTN: DRCMA-EE 5001 Eisenhower Ave Alexandria, VA 22333
1	CDR, US Army Materiel Development and Readiness Command ATTN: DRCRD-FW 5001 Eisenhower Ave Alexandria, VA 22333
1	Commander US Army Training & Doctrine Cmd ATTN: ATCD-F Fort Monroe, VA 23651
1	Commander US Army Missile Research & Development Command ATTN: DRSMI-RR, Dr. J. P. Hallowes Redstone Arsenal, AL 35809
1	Commander US Army Armament Research and Development Command ATTN: DRSAR-RDP (Library) Rock Island, IL 61201

No. Copies	Addressee
3	Commander US Army Combined Arms Combat Developments Activity ATTN: ATCAIC-IE Fort Leavenworth, KS 66027
1	Commander US Army Logistics Center ATTN: ATCL-MA Fort Lee, VA 23801
1	Commandant US Army Ordnance School ATTN: ATSOR-CTD Aberdeen Proving Ground, MD 21005
1	Commander US Army Intelligence School ATTN: ATSIT-CTD Fort Sill, OK 73503
1	Commandant US Army Engineer School ATTN: ATSE-CTD-DT-TL Fort Belvoir, VA 22060
1	Commander Picatinny Arsenal ATTN: SARPA-TS-S #59 Dover, NJ 07801
1	Commander Frankford Arsenal ATTN: (Dr. Wm. McNeill) PDS Philadelphia, PA 19137
1	Commander USASA Test & Evaluation Center Fort Huachuca, AZ 85613
1	US Army Research Office-Durham ATTN: CRDARD-IP Box CM, Duke Station Durham, NC 27706
1	US Army Research Office-Durham ATTN: Dr. Robert J. Lontz Box CM, Duke Station Durham, NC 27706
1	Commander HQ MASSTER Technical Information Center ATTN: Mrs. Ruth Reynolds Fort Hood, TX 76544

No. Copies	Addressee
1	USA Security Agency ATTN: IARD Arlington Hall Station Arlington, VA 22212
1	Commander US Army Tank-Automotive Research and Development Command ATTN: DRSTA-RW-L Warren, MI 48090
1	Commandant US Army Air Defense School ATTN: C&S, Dept, Msl Sci Div Fort Bliss, TX
1	Commander US Army Combined Arms Combat Development Activity ATTN: ATCACC Fort Leavenworth, KS 66027
2	Commander US Army Yuma Proving Ground ATTN: STEYP-MTD (Tech Lib) Yuma, AZ 85364
1	Commander US Army Arctic Test Center ATTN: STEAC-PL APO Seattle, 98733
1	CO, US Army Tropic Test Center ATTN: STETC-MO-A (Tech Lib) Drawer 942 Fort Clayton, Canal Zone 09827
1	Commander US Army Logistics Center ATTN: ATCL-MC Fort Lee, VA 22801
1	Directorate of Combat Developments US Army Armor School ATTN: ATSB-CD-AA Fort Knox, KY 40121
1	Commandant US Army Inst for Military Assistance ATTN: ATSU-CTD-OMS Fort Bragg, NC 28307
1	Commander US Army Missile Research and Development Command ATTN: DRSMI-RE (Mr. Pittman) Redstone Arsenal, AL 35809

No. Copies	Addressee
1	Commander US Army Systems Analysis Agency ATTN: DRXSY-T (Mr. A. Reid) Aberdeen Proving Ground, MD 21005
1	Commandant US Army Signal School ATTN: ATSN-CTD-MS Fort Gordon, GA 30905
1	Commander US Army Tank-Automotive Research and Development Command ATTN: DRSTA-RHP, Dr. J. Parks Warren, MI 48090
2	NASA Scientific & Tech Info Facility ATTN: Acquisitions Br (S-AK/DL) P.O. Box 33 College Park, MD 20740
2	Advisory Group on Electron Devices 201 Varick Street, 9th Floor New York, NY 10014
1	Ballistic Missile Radiation Anal Ctr Env Research Inst of Michigan Box 618 Ann Arbor, MI 48107
2	Chief Ofc of Missile Electronic Warfare Electronic Warfare Lab, ECOM White Sands Missile Range, NM 88002
1	Chief Intel Materiel Dev & Support Office Electronic Warfare Lab, ECOM Fort Meade, MD 20755
2	Commander US Army Electronics Research and Development Command ATTN: DRSEL-MS-TI Fort Monmouth, NJ 07703
1	TACTEC Battelle Memorial Institute 505 King Ave Columbus, OH 43201
1	Commander US Army Electronics Research and Development Command ATTN: DRSEL-PT-ST Fort Monmouth, NJ 07703

No. Copies	Addressee
1	Study Center National Maritime Research Center ATTN: Rayma Feldman King's Point, NY 11024
20	Director US Army Night Vision and Electro- Optics Laboratory ATTN: Byong H. Ahn Fort Belvoir, VA 22060
1	Director The Charles Stark Draper Laboratory ATTN: Byong-ho Ahn 555 Technology Square Cambridge, MA 02139

4 -90,052—AG—Ft Belvoir